Chapter 3

Enclosure of Sodium Tetrahydroborate ($NaBH_4$) in Solidified Aluminosilicate Gels and Microporous Crystalline Solids for Fuel Processing

Josef-Christian Buhl, Lars Schomborg and Claus Henning Rüscher

Additional information is available at the end of the chapter

http://dx.doi.org/10.5772/50186

1. Introduction

The development of new materials for production and high storage capacities is most essential for an efficient use of the future energy source "hydrogen". Besides cryogenic and high pressure storages several chemical alloys like metal hydrides, carbon nanotubes or clathrates have been discussed [1-5]. New metal-organic framework compounds (MOFs) have been developed and proved to be outstanding hydrogen storage materials [6-9]. Besides these new materials also the well known hydride salt sodium tetrahydroborate ($NaBH_4$) has recently been moved into new centre of interest as a possible hydrogen source according to its large hydrogen capacity, 5.3 wt% H_2, which could be used to gain 2.4 l H_2/g $NaBH_4$ in the reaction with water [10-13].

Our recent studies succeeded in an easy and safe way of handling $NaBH_4$ salt in strong alkaline aluminate and silicate solutions. Brought together gelation occurs immediately which could be further solidified by drying [14]. There remains a heterogeneous solid containing $NaBH_4$ crystals and sodalite-type nanocrystals which are "glued" together in a matrix formed by short range ordered Si-O-Al (sialate) bonds. This new compound exhibits a high capacity of up to 72 wt% of $NaBH_4$ which could easily be handled in moisture atmosphere without any segregation or loss of $NaBH_4$ for weeks [15]. The complete amount of $NaBH_4$ inserted during synthesis could be used for the hydrogen production controlled by pH-value with the addition of weak acid solution. Details about synthesis of the gel, alteration during solidification and quantification of hydrogen storage capabilities will be described here in section 2.

Section 3 follows another idea of the enclathration of $NaBH_4$ into a zeolite framework structure which prevents the BH_4-anion from hydrolysis and offers a safe and specific way of hydrogen release in a rather controlled way. In [16] Barrer suggested an impregnation of pre-formed zeolites like X and Y with boronhydride salts like $Al(BH_4)_3$ or $NaBH_4$. Some experiments in this direction will also be demonstrated here, showing, that the BH_4-anion cannot be stabilized in such types of matrixes (section 3.1). Contrary to this the incorporation of BH_4-anions into the small sodalite cages during the formation of the sodalite crystals succeeded in a direct way of hydrothermal synthesis [17-21]. By this method $NaBH_4$-sodalites with aluminosilicate, gallosilicate and aluminogermanate framework compositions could be prepared (section 3.2) and a detailed understanding of their structure could be worked out (3.3). Further investigations succeeded in variations of crystal sizes between typically obtained microcrystals and nanocrystalline material also showing details of their hydrogen release reactions [22, 23]. The state of the art of a control of hydrogen release reactions of the BH_4-anions in the sodalite crystals in consecutive reaction steps with water will be outlined for the microcrystalline aluminosilicate sodalite (section 4.1). Indications of back reaction of the pre-reacted BH_4-anion in the sodalite cage were also reported [24, 25]. The realization of direct reinsertion of hydrogen in reacted $NaBH_4$ is ruled out so far, which makes its global use as energy storage so problematically. However, this problem could be overcome for the BH_4-anion in the sodalite cages. Thus we report in section 4.2 our results realizing first steps of hydrogen reinsertion into pre-reacted BH_4-sodalite.

2. Synthesis and characterisations of $NaBH_4$ crystals grown in an aluminosilicate gel

2.1. Solidified $NaBH_4$ aluminosilicate gel and its partial crystalline secondary products

The new material is a gel, formed from sodium-tetrahydroborate ($NaBH_4$), sodium-silicate, sodium-aluminate and water with the chemical composition 3 Na_2O : 2 SiO_2 : Al_2O_3 : 9-18 $NaBH_4 \cdot x\ H_2O$; $0 < x < 112$. The material can be obtained by a two-step reaction process. Firstly an aluminosilicate mixture under addition of high portions of $NaBH_4$ has to be prepared at room temperature. Secondly this mixture has to be dried by heating between 80 and 110°C between 0.5 and 4 h. During this procedure the gel undergoes a partial stepwise alteration resulting in solidification of the final product. As an example a typical synthesis batch can easily be prepared by dissolving $NaAlO_2$ (Riedel-de Haen 13404) in 1.5 ml H_2O before high $NaBH_4$ amounts (between 100 - 850 mg) have to be added to this solution and dissolved under stirring until a clear solution arises (solution I). A second solution is prepared from 310 mg Na_2SiO_3 (Fluka 2299129) and 1.5 ml water. After total dissolution of the silicate the same amount of $NaBH_4$ as used for preparation of solution I is added and the mixture has to be stirred too, until a clear solution has formed (solution II). Afterwards gel precipitation starts by the dropwise addition of solution II to solution I. A pasty liquid

results from this alkaline gel-boranate mixture. After this the gel is exposed to drying procedure in an oven as described above.

Directly after precipitation of the $NaBH_4$ gel the product has the state of an amorphous sodium aluminosilicate, containing the whole amount of BH_4-anions from the inserted sodium-tetrahydroborate. As a result of separation of NaOH during gel precipitation and alteration process, the alkalinity remains very high, thus preventing the tetrahydroborate from decomposition by hydrolysis. The subsequent process of drying at 80°C up to 110°C between 0.5 h and 4.0 h causes rapid gel hardening. According to this solidified aluminosilicate gels are converted into secondary products with a high content of $NaBH_4$. Gel precipitation and alteration during drying at 110°C up to two hours was followed by X-ray powder diffraction as shown in Fig. 1. The powder diagram of the pure salt $NaBH_4$ is inserted in Fig. 1 for comparison.

It can be seen that without further drying at enhanced temperature only short range order could be present revealing a very broad peak around 30° 2 Theta (d = 2.97 Å) and a shoulder around 48° 2 Theta. The broad peak could be related to short ranged ordered

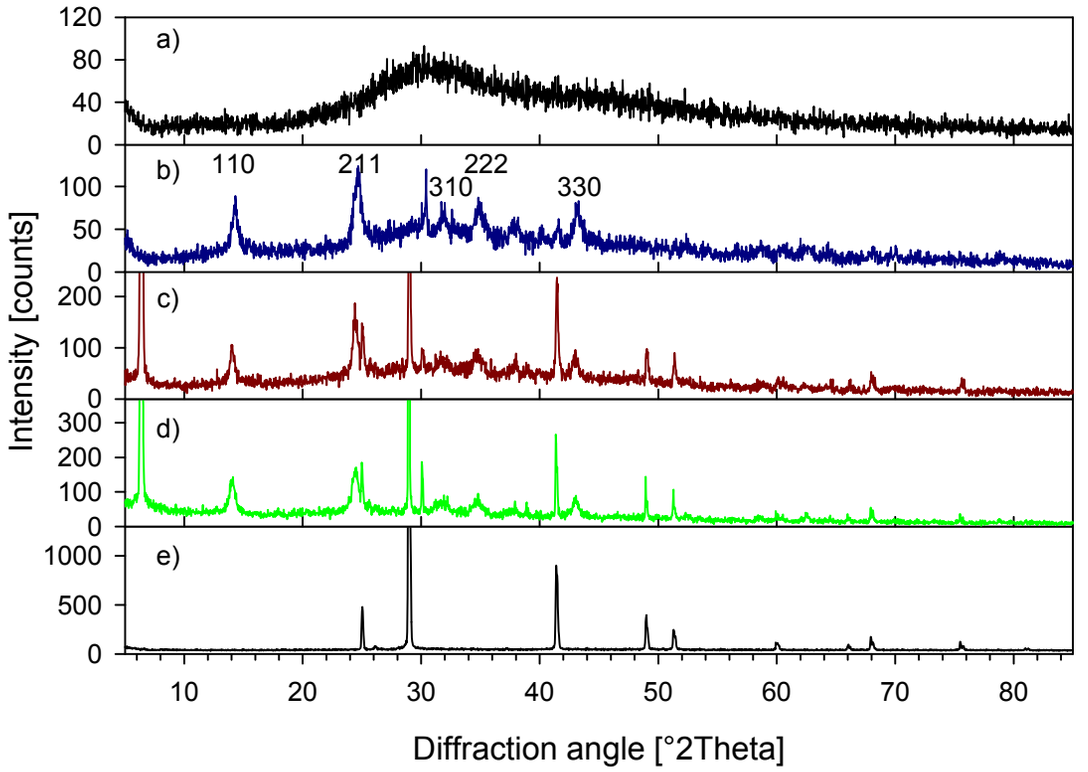

Figure 1. X-ray powder patterns of $NaBH_4$ - gel in dependance oft the drying period during drying at 110°C: directly after gel precipitation (a) and after drying for 0.5 h (b), 1.0 h (c) and 2.0 h (d). The pattern of the pure $NaBH_4$ salt dried at 110°C, is inserted for comparison (e).

Si-O-Al (sialate) type bonds which are typically also observed in geopolymers, i.e. when a mixture of water glass and metakaolin is aged [26]. A significant crystallization can be seen after 30 minutes of drying, reducing significantly the amount of short ranged ordered Si-O-

Al bonds. The four most intensive peaks can uniquely be indexed as (110), (211), (310), (222) and (330) within a sodalite framework. Further aging at 110°C does not alter the sodalite type peaks, which remain rather broad (Fig. 1 c, d). However, the intensity related to short range ordered sialate bonds becomes strongly reduced simultaneously with the appearance of a rather sharp diffraction peak at 6.5° 2 Theta (d = 13.66 Å). The initial crystallisate in the aluminosilicate could be identified as sodalite type nanocrystals. The strong and sharp peak at 6.5° 2 Theta (13.66 Å) in the XRD pattern (Fig. 1) could be related to a "disordered" sequence obtaining a 1.5· a superstructure, a = typical lattice parameter of the sodalite. The structure may not be seen as an intermediate between sodalite and cancrinite [27]. Parallel to this growth of a sodalite type aluminosilicate the $NaBH_4$ phase re-crystallizes. This process of $NaBH_4$-recrystallization under the strong alkaline conditions within the solidified aluminosilicate gel can be seen according to the evaluation of the $NaBH_4$ peaks in agreement with data of PDF-9-386. Thus the complete material can be regarded as a composite material containing $NaBH_4$ and sodalite-type phase embedded in or glued together by sialate bonds

A SEM photograph of the $NaBH_4$ gel, exposed to open conditions for 4 weeks is given in Fig. 2. Some more general features may be described for the handling of the $NaBH_4$-gel under open conditions. XRD pattern taken in a series up to 4 weeks are shown in Fig. 3. Compared with the powder pattern taken directly after precipitation and drying for two hours, after 10 days held under open conditions no remarkable decomposition occurs. According to the alkalinity of the sample some sodium carbonate was formed by uptake of carbon dioxide from the air. This can be seen by weak additional lines in the powder pattern, consistent with Na_2CO_3 PDF-18-1208. After 4 weeks under open conditions the intensity of all diffraction peaks becomes reduced and the samples gain a paste-like character.

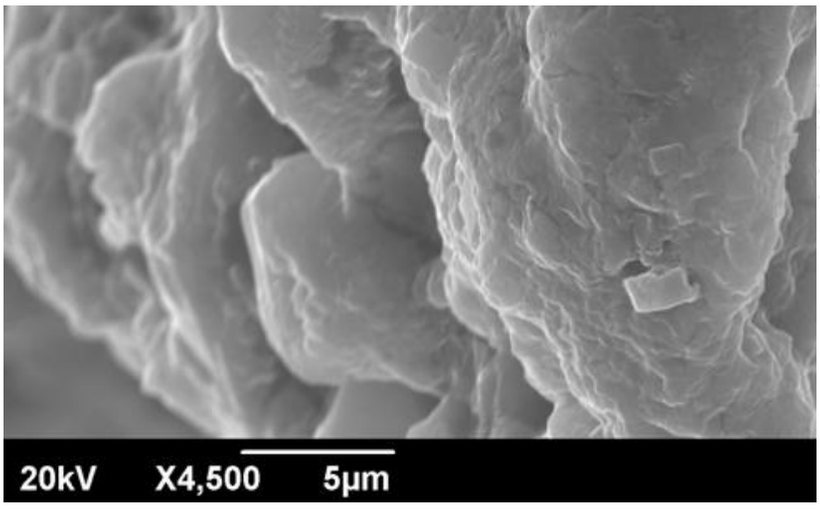

Figure 2. Scanning electron microscopy of $NaBH_4$ gel held for 4 weeks under open conditions and EDX area analysis.

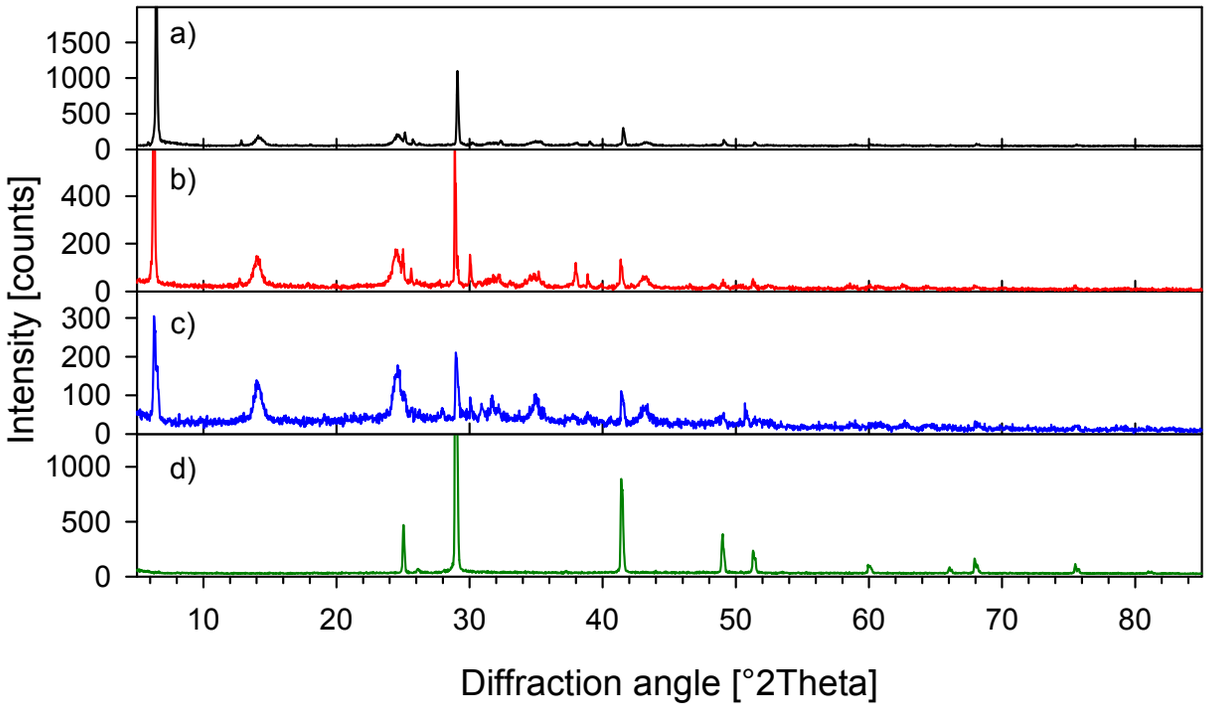

Figure 3. XRD investigation of the stability of $NaBH_4$-gel under open conditions: a) directly after precipitation and drying for two hours, b) after 10 days, held under open conditions and c) after 4 weeks under open conditions. The pattern of pure $NaBH_4$-salt (dried at 110°C) is included for comparison (d).

The samples were further analysed by infrared (IR) absorption spectroscopy (KBr method). The tetrahedral BH_4-anion groups of the $NaBH_4$ crystals could be identified by strong vibration modes at 1143 (ν_4), 2286 (2 ν_4), 2241 (ν_3) and 2390 ($\nu_2+\nu_4$) ([28-31], and more recently [32]) as shown in Fig. 4. By comparison with the spectrum of $NaBH_4$ the peaks related to the $NaBH_4$ in the aluminosilicate gel can be identified at the same positions in spectra a-d.

A significant uptake of water molecules to the gel could be seen as indicated by the increasing intensity of the peak at 1630 cm^{-1} (H_2O bending) and the main peak around 3500 cm^{-1} together with the broad shoulder towards lower wavenumbers. Despite this uptake of water no sign of hydrolysis reaction accompanied by formation of other borate species [33-35] at the expense of $NaBH_4$ can be derived from the spectra. This is a further indication for the stability of the $NaBH_4$ in the composite material. The peak at around 1450 cm^{-1} and the smaller one at 880 cm^{-1} indicate the presence of CO_3^{2-}anions [36, 37]. As already mentioned, formation of sodium carbonate is the result of reaction with CO_2 from the air under alkaline conditions on the gel surface. Indications of the presence of sodalite framework are given by the small peaks at 436 and 469 cm^{-1}, the triplicate peak at 668, 705 and 733 cm^{-1} and the contribution at 990 cm^{-1} as could be realized by comparison with a typical sodalite spectrum Fig. 4. The sodalite spectrum appears to be superimposed to what has been called geopolymer type matrix, i.e. the alumosilicate gel. Similar spectra were observed during in situ investigations of sodalite crystallization from appropriate alumino-silicate gel in a KBr matrix [38].

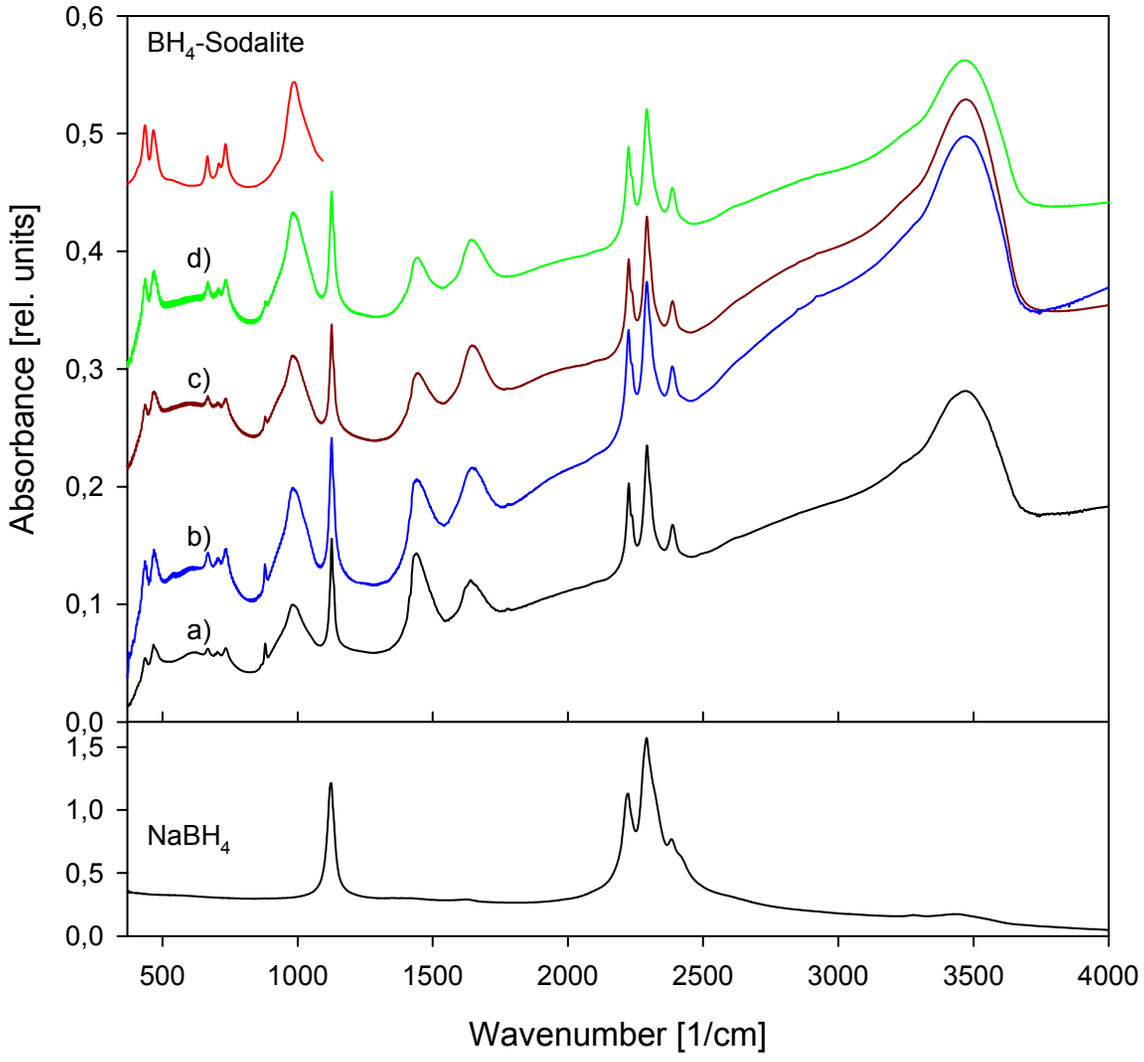

Figure 4. IR-absorption spectra of a series of $NaBH_4$-gel: directly after precipitation and drying for 2 h at 110°C (a); sample after 1 week (b), 3 weeks (c) and 4 weeks (d). Spectra b-d were normalized to spectrum a related to the BH_4-absorption intensity for better comparison. An example of typical as prepared BH_4-Sodalite is also shown.

Further tests of thermal stability of the new composite material including $NaBH_4$ crystals were carried out for heating the sample in a muffle furnace under open conditions in air. Spectra obtained before the treatment and treated for 2 h at 100°C steps up to 500°C are given in Fig. 5 (a-e). It can be seen that the $NaBH_4$ in the gel largely remains stable up to 300°C and then starts to decompose into borate species at temperatures between 300 and 400°C in air. A simple test of hydrogen release could be given by burning the sample initiated with a pocket lighter. The sample is burning and a glassy-like mixture of aluminosilicate and sodiumborate remains as could be identified in the IR absorption spectra, also shown in Fig. 5 (f). A more precise way for hydrogen release is the reaction in acid solutions [39]. The investigation of hydrogen release from solidified aluminosilicate gels by wetting with diluted acid is described in the following.

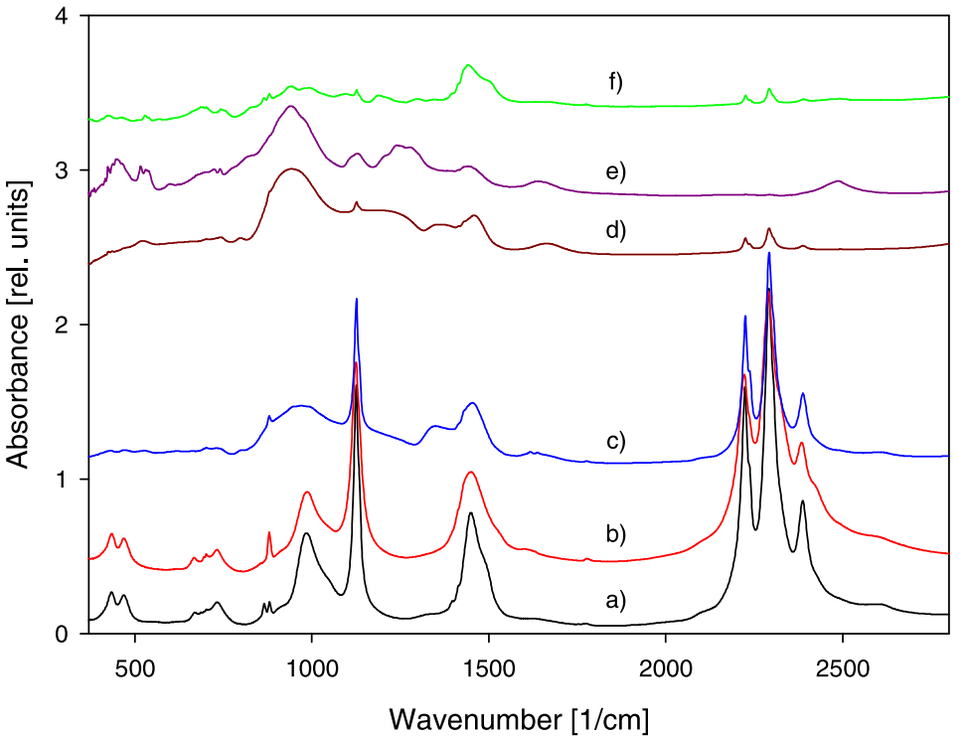

Figure 5. IR-absorption spectra of $NaBH_4$-gel heated in a muffle furnace for 2 h at 100°C (a), 200°C (b), 300°C (c), 400°C (d), 500°C (e) and of a sample after burning (f).

2.2. Hydrogen release experiments and further optimizations of storage capability

Hydrogen release experiments and optimizations of the starting compositions and solidification conditions for the hydrogen storage capability were carried out using an apparatus made from glassware as shown in Fig. 6. It consists of a 100 ml bulb, a gas syringe which measures the volume expansion related to the gas release, and the possibility of injection of liquid reactants. The bulb could also be heated and the temperature inside the bulb could be measured during the experiment. A stability check of the $NaBH_4$ enclosed in the aluminosilicate gel may be given in comparison to the raw $NaBH_4$-salt. Below 40°C $NaBH_4$ creates a stable hydrated form $NaBH_4 \cdot 2H_2O$ in contact with water. This species dehydrates at about 40°C to water and $NaBH_4$ which leads to the uncontrollable reaction with water [32]. For a further check of the reactivity of $NaBH_4$-salt with water an amount of 26.2 mg of $NaBH_4$ was wetted with 10 ml water in the bulb and heated to 70°C. This reveals an increased gas volume to about 58.7 ml in the reaction with water. For 10 ml water in the repeated experiment the gas volume increased by about 21 ml as a reference value. Since the amount of 26.2 mg $NaBH_4$ could release 58.66 ml of hydrogen, as also verified in further experiments below Fig. 7, it could be estimated that about 58% of the $NaBH_4$ reacted at 70°C under such conditions. Repeating the same experiment for an example of aluminosilicate gel (the $NaBH_4$-gel_0.47, Fig. 7, Tab. 1) reveals that only 11% of the $NaBH_4$ enclosed in the gel reacted. This shows a significant increase in protection.

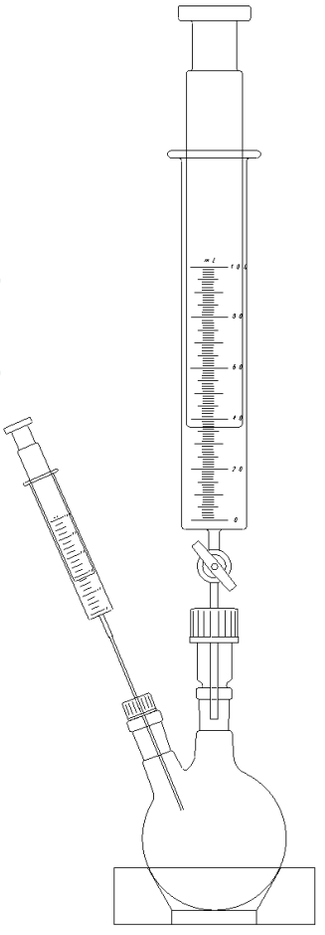

Figure 6. Apparatus as used for measuring gas release

A controlled hydrogen release from the $NaBH_4$ enclosed in the aluminosilicate gel could be achieved by lowering the pH-value by adding diluted acid. Using an injection needle as sketched in Fig. 6 diluted acid was added through a pierceable rubberplug, so the apparatus remained gas tight. The released gas was identified as hydrogen using the hydrogen-oxygen-reaction. Due to the high alkaline character of the $NaBH_4$-gel CO_2 from the surrounding air is absorbed in small amounts as CO_3^{2-} (compare IR-Spectra Fig. 4). By adding the diluted acid the CO_2 is also released. A gas check showed, however, that the concentration of CO_2 was below the detection limit of 1000 ppm and therefore negligible. As diluted acid a 1 % solution of hydrochlorid acid was chosen. It showed the best compromise between needed volume for entire hydrogen release and reaction velocity. If higher concentrations of acid were used the gas is released too fast. To get reliable results for every gel composition at least 5 different sample masses were investigated. The volumes of added acid were subtracted from the shown volume at the gas syringe to get the pure released gas volumes. The volumes obtained were plotted for the different samples against the used sample mass. With a linear regression the volume of released hydrogen per 100 mg sample could be calculated and compared to the pure $NaBH_4$ salt Fig. 7, Tab. 1.

$NaBH_4$/solid ratios between 0.26 and 0.75 were investigated. Tab. 1 depicts the synthesis masses of the investigated samples. The experiments show a linear trend between used sample mass and released hydrogen volume (Fig. 7). The more $NaBH_4$ is enclosed in the aluminosilicate gel the more hydrogen can be stored. Using a $NaBH_4$/solid ratio of 0.75 at the synthesis the released hydrogen volume is equivalent to 72 % of the pure $NaBH_4$-salt. More added $NaBH_4$ during the synthesis lowers the protection ability of the aluminosilicate gel after solidification. The hydrogen content approaches a saturation with further added $NaBH_4$ mass during synthesis. Some higher amount could still be enclosed by decreasing the solidify temperature. This was investigated using $NaBH_4$/gel ratios of 0.47 and 0.59. At 80°C solidified samples the 0.59 $NaBH_4$-gel releases about 15 % more hydrogen compared to the identical synthesis, solidified at 110°C. This higher amount of hydrogen storage capacity is reached, however, at the expense of longer solidify time up to 48 hours. Drying temperatures below 40°C are not able to solidify the $NaBH_4$-gel even after 96 hours which makes these temperatures inefficient. Below 40°C the hydrogen release per sample mass is very low because main fractions of the sample mass consist of water.

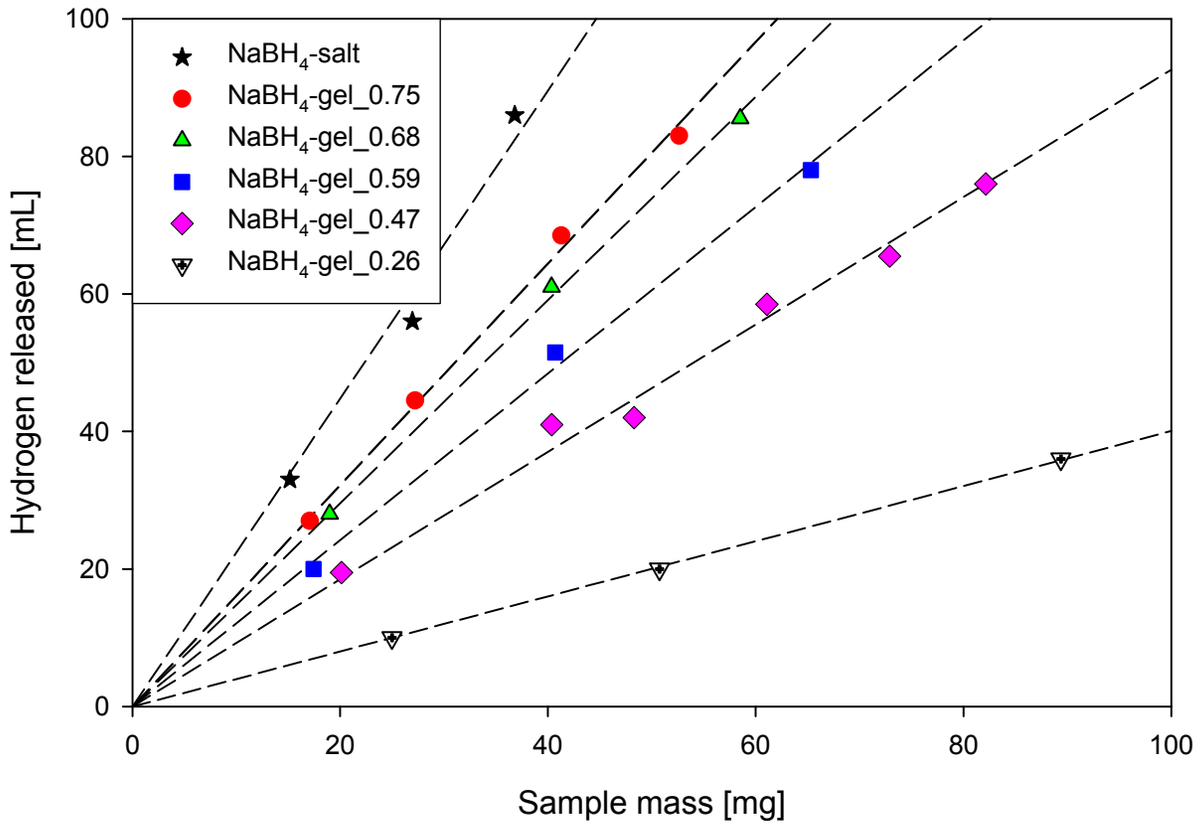

Figure 7. Released gas volume related on sample mass by the reaction of $NaBH_4$-gel of various ratios $NaBH_4$/gel as denoted with diluted hydrochloric acid. The results using pure $NaBH_4$-salt are also shown. Dashed lines result from linear regressions to the data.

Sample name	$NaBH_4$ [mg]	Na_2SiO_3 [mg]	$NaAlO_2$ [mg]	R	ST [°C]	H_2/100mg [ml]	H_2/H_2 from $NaBH_4$-salt [%]
$NaBH_4$-salt	-	0	0	1	-	224(exp.) 240 (lit.)	100
gel_0.26	200	310	250	0,26	110	40	17,86
gel_0.47	500	310	250	0,47	110	92	41,07
gel_0.47_80	500	310	250	0,47	80	106	47,32
gel_0.47_40	500	310	250	0,47	40	94	41,96
gel_0.47_18	500	310	250	0,47	18	55	24,55
gel_0.59	800	310	250	0,59	110	121	54,02
gel_0.59_80	800	310	250	0,59	80	143	63,84
gel_0.68	1200	310	250	0,68	110	148	66,07
gel_0.75	1700	310	250	0,75	110	161	71,88

Table 1. Used reactants and results of hydrogen release. Column 1-3: the used amounts of reactants (solids) for gel preparation (in mg); column 4: the ratio R =$NaBH_4$/solid; column 5 solidify temperature ST (°C) ; column 6: H_2/100 mg = hydrogen released per 100 mg sample (in ml) from linear regression to data Fig. 7); column 7: H_2/H_2 from $NaBH_4$-salt.

It can be concluded that the hydrogen content of the solidified aluminosilicate gels can be varied with the amount of added $NaBH_4$ during the synthesis. Till now the highest ratio of $NaBH_4$ per solid reactants in the synthesis is about 0.75 of gels solidified at 110°C. Some higher amount could still be enclosed decreasing the solidify temperature, however, on extension of the solidification time.

3. The BH_4-anion enclosed in cages of the sodalite

In addition to the materials like carbon nanotubes or MOFs as well as the aluminosilicate gel, zeolites could be suitable matrices for inclusion of hydrogen because of their open framework structures. Hydrogen loading into zeolite cavities under high pressure has been discussed. It could be shown that the sodalite structure could exhibit a high storage capacity but requires a loading temperature of 300°C and a pressure of 10 MPa [40]. A completely different way has been discovered more recently by direct enclosure of the BH_4-anion in the sodalite cage during soft chemical synthesis under hydrothermal conditions [17, 18]. The enclathration of one BH_4-anion into each of the sodalite cages prevents the anion from hydrolysis and offers a safe and specific way of hydrogen release as will be described in detail below. Barrer proposed in his outstanding work [16] an impregnation of pre-formed zeolites like A, X and Y with boronhydride salts like $Al(BH_4)_3$ or $NaBH_4$. However, the incorporation of hydride-anions into the small sodalite cage type units in a post-synthesis step seems impossible due to the diameter restrictions of the six ring window. Some primary attempts of direct synthesis of zeolites like LTA with $NaBH_4$-filled toc-subunits may be shown to be unsuccessful and LTA can only be obtained in mixtures with BH_4-sodalite.

3.1. Primary steps

The three-dimensional structure net of the sodalites is known for more than 80 years [41]. It was found as basic structure type of many zeolite related compounds up to date [42]. The general sodalite composition is $Na_8[T^1T^2O_4]_6X_2$ where T^1 is a trivalent cation (usually Al^{3+}) and T^2 a tetravalent cation (usually Si^{4+}) but others like Ga^{3+} and Ge^{4+} can be built in during synthesis [18, 43-45]. The sodalite framework is built up by a space filling package of truncated octahedral cages ("toc-units") formed by tetrahedral TO_4 units. Each cage is filled by a $[Na_4X]^{3+}$ -complex with X representing a monovalent anion or anion group as for example the BH_4-anion. Those guests are enclathrated during synthesis according to the chlathralite like properties of sodalites [46]. As known for other salt-filled sodalites the thermal reactivity of the enclathrated guests can differ from the behaviour of the pure salt according to special interactions of the guest-complex with the sodalite host-framework [47-50]. The toc-unit of the sodalite structure is a common building unit in other zeolites like LTA, LSX, X and Y. Fig. 8 gives a schematic view on the sodalite framework and the framework of zeolite LTA.

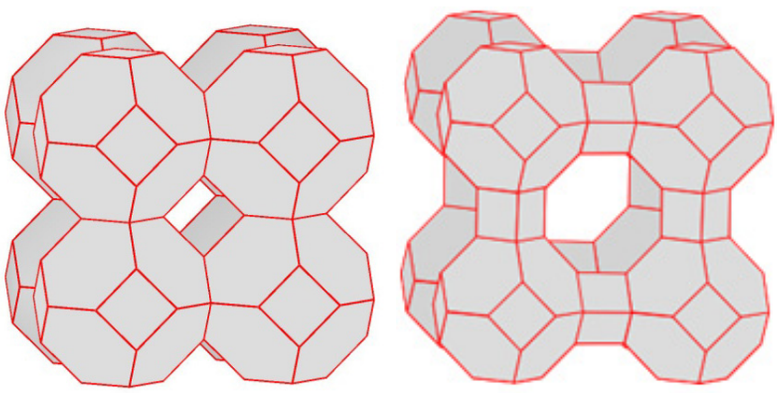

Figure 8. Structure scheme of frameworks of sodalite (left) and zeolite LTA (right).

With the aim to clarify major questions connected with wet chemistry of $NaBH_4$ and zeolites with wider open frameworks than sodalites, experiments on impregnation possibility by interaction of zeolite A (LTA) and $NaBH_4$ and on direct synthesis of $NaBH_4$-LTA using the gel method under addition of $NaBH_4$ were carried out. The impregnation experiments were performed using commercial zeolite Na-LTA (Fluka-69836) and $NaBH_4$. The zeolite was stirred in 2 M NaOH-$NaBH_4$ solution at room temperature with a solid:liquid ratio of 1:20. After a treatment period of 60 minutes the solution was filtered. NaOH residues were carefully washed out of the solid followed by drying at 80°C over night. However the IR absorption spectrum does not show the presence of any BH_4-anions in the otherwise typical LTA zeolite signatures. Therefore, it can be concluded that the $NaBH_4$ salt or BH_4-anions do not enter or cannot be stabilized neither in the supercages (grc) nor in the toc units of LTA.

Because of this failure of BH_4-incorporation into the cavities of pre-formed zeolite LTA another experimental series was performed to test possibilities of direct formation of $NaBH_4$-LTA. The common gel method was used under addition of $NaBH_4$ salt to the gel

during its precipitation. Sodium metasilicate and sodium aluminate were used for gel formation and $NaBH_4$ salt was added to both of the starting solutions before they were mixed to form the gel. Whereas the sodalite crystallization occurs under high alkalinity which prevents rapid hydrolysis of the inserted BH_4-anion, LTA formation needs lower alkaline solutions. Thus the experiments were performed under the Na_2O:H_2O- ratio of 1:20 M. Under those conditions of low alkalinity a partial decomposition of $NaBH_4$ cannot be excluded. Therefore the crystallization time was shortened neglecting an otherwise necessary further gel aging step in order to prevent $NaBH_4$ decomposition choosing a temperature of 100°C for 2-4 h. This higher temperature for LTA formation was selected to also accelerate the crystallization process within the short crystallization time interval.

The X-ray powder pattern of a typical synthesis product is shown in Fig. 9. The powder patterns of common zeolite LTA (Fluka) and $NaBH_4$-sodalite are inserted in this figure for comparison. Beside sharp peaks, consistent with the powder pattern of zeolite LTA, broad lines of sodalite can be distinguished from the powder pattern of the synthesis product.

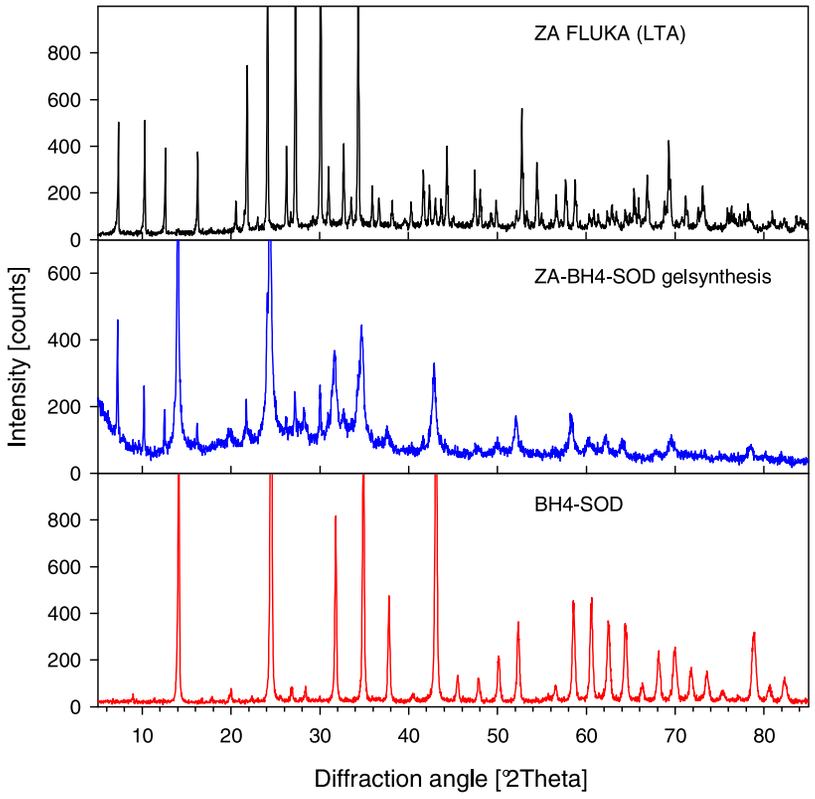

Figure 9. X-ray powder patterns of: product of direct synthesis in the LTA-$NaBH_4$ system at 100°C and 4 h synthesis time (pattern in the middle) and of common zeolite LTA-Fluka (on top) and $NaBH_4$-sodalite (bottom).

According to this, the product can be regarded as a mixture of a lower amount of zeolite LTA and mainly nano-sized sodalite beside some short range ordered aluminosilicate units, indicated by the broad peak in the range 20° to 40° 2 Theta. The formation of the two phases zeolite LTA and sodalite can also be observed in the IR absorption spectrum in comparison

to spectra of the $NaBH_4$-sodalite and zeolite LTA (Fluka) Fig. 10. In particular the sodalite can be identified by the triplicate sodalite "fingerprint".

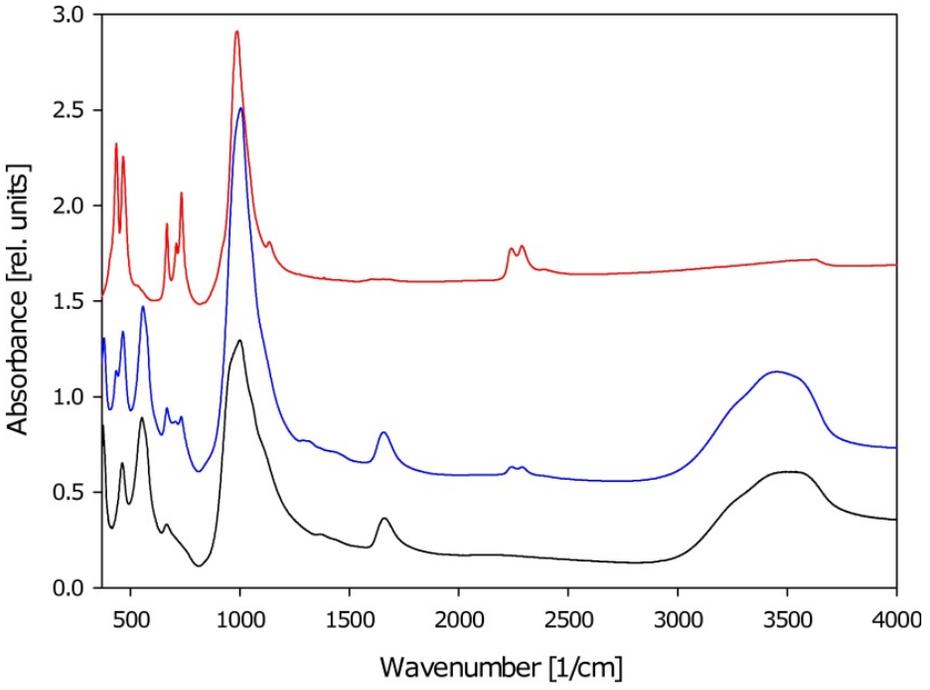

Figure 10. FTIR-spectra of BH_4-SOD, two phase product of the direct synthesis experiment and the spectrum of zeolite LTA-FLUKA; (spectra from top to bottom).

Further experiments under variation of the alkalinity, the solid/liquid ratio as well as the time of syntheses all failed to obtain $NaBH_4$ zeolite LTA. In each case a two phase product was observed, consisting of $NaBH_4$ sodalite and $NaBH_4$-free zeolite LTA. The reaction parameters mentioned here showed only a small influence on the mass ratio of both of these phases. The results are a hint that even a direct crystallization of $NaBH_4$-zeolite LTA seems to be impossible under the conditions of gel-crystallization usually used in zeolite chemistry.

3.2. Enclosure of the BH_4-anion in micro- and nano-crystalline sodalites

The route of synthesis follows certain rules in order to include the BH_4-anion in the sodalite cage and not to obtain just co-crystallization of $NaBH_4$ and the sodalite within the aluminosilicate matrix as described in section 2. Synthesis of $NaBH_4$-aluminosilicate sodalite in microcrystalline form was performed under mild hydrothermal and strong alkaline conditions (NaOH) using kaolinite as Si-Al-source. An excess of $NaBH_4$ salt has to be added to this solution. From wet chemical reaction behaviour of pure sodium tetrahydroborate in water it is known that the kinetics of decomposition are highly influenced by the alkalinity [51, 52, 10]. Further parameters of synthesis like the solid to liquid ratio, temperature and reaction time had to be optimized for sodalite synthesis with hydrolysis sensitive BH_4-anions. 50 ml Teflon coated steel autoclaves were used for synthesis.

After screening experiments the amounts of 1 g of kaolinite, 2 g of sodium tetrahydroborate salt and 10 ml of 16 M sodium hydroxide solution were selected for preparation of the

favored reactant mixture. Crystallization was performed at a temperature of 110°C for 24 hours reaction time. The final products were washed with water and dried at 80°C for 24 hours [17]. Tetrahydroborate-sodalite nanoparticles were successfully synthesized even at lower temperature hydrothermal conditions (60°C) from high alkaline aluminosilicate gels and $NaBH_4$ salt [22, 23]. Preparation of basic hydrosodalite by this very simple method was first described by [53, 54] during experiments on zeolite A crystallization at very low temperatures under superalkaline conditions. Fine tuning of this gel method by [55] also yielded basic-hydrosodalite nanoparticles. Gel conditions are suitable for precipitation of salt-filled sodalites and cancrinites, too, as recently demonstrated by [56, 57] for the nitrate sodalite-cancrinite system. The use of similar gels at low temperatures under superalkaline conditions was shown to be a suitable method for $NaBH_4$-sodalite nanoparticle formation [22, 23] as the hydrolysis reaction of the highly moisture sensitive $NaBH_4$ salt is retarded under low temperature strong alkaline conditions [10, 51, 52, 58].

Details for obtaining BH_4-sodalite nanoncrystalline samples are batch compositions 13 Na_2O : 2 SiO_2 : 1,5 Al_2O_3 : 5 $NaBH_4$: 220 H_2O prepared from analytical grade chemicals sodium-metasilicate, sodium aluminate, $NaBH_4$ and sodium hydroxide solution. Syntheses were performed in a Teflon coated steel autoclave at 60°C. The final products were washed with 500 ml water and dried at 110°C for 48 h [22, 23]. A heating period of 12 h was proved to be an optimal reaction time for nanoparticle formation of suitable size and sufficient crystallinity.

The gallosilicate tetrahydroborate enclathrated sodalite was prepared by alkaline hydrothermal treatment of a solid mixture of gallium oxide, sodium silicate, $NaBH_4$ in 10 ml of a 6 M NaOH at 110°C for 24 h, using teflon lined autoclaves. The final product was washed with water and dried at 80°C for 24 hours [18]. Synthesis of the aluminogermanate phase was performed from a beryllonite analogous $NaAlGeO_4$ following [59]. This starting material was obtained from GeO_2, γ-Al_2O_3 and Na_2CO_3 heated for 12 h at 1200°C before quenched to room temperature and crystallized at 800°C for 48 hours. The sodalite was subsequently synthesized by treatment of the $NaAlGeO_4$ in 10 ml 4 M NaOH at 110°C for 24 hours, again using a Teflon lined autoclave and same washing procedure as for the gallosilicate sodalite [18].

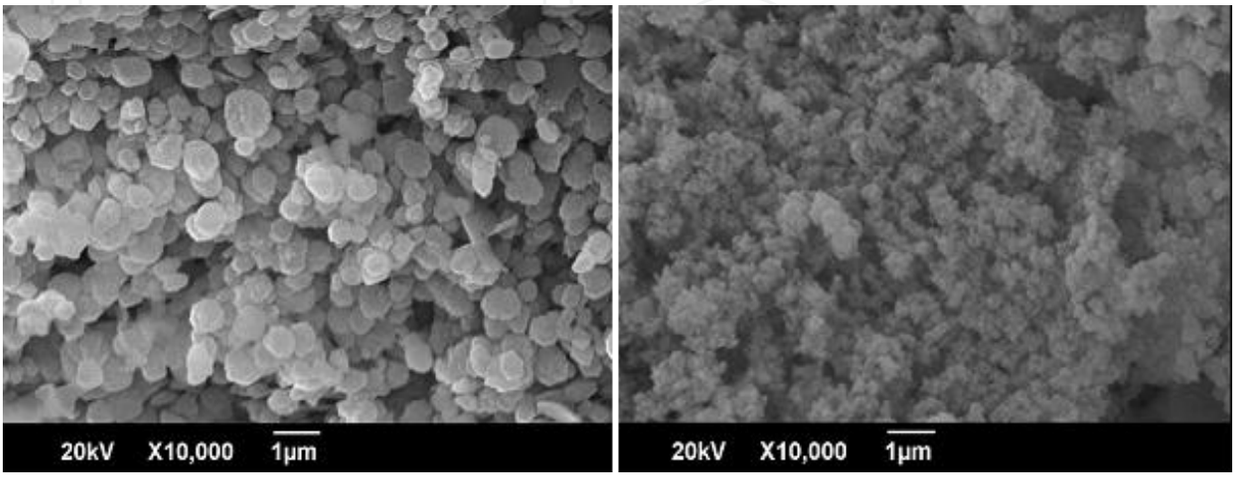

Figure 11. SEM-image of the microcrstalline sample (left) and the nanocrystalline product of the 12h experiment (right).

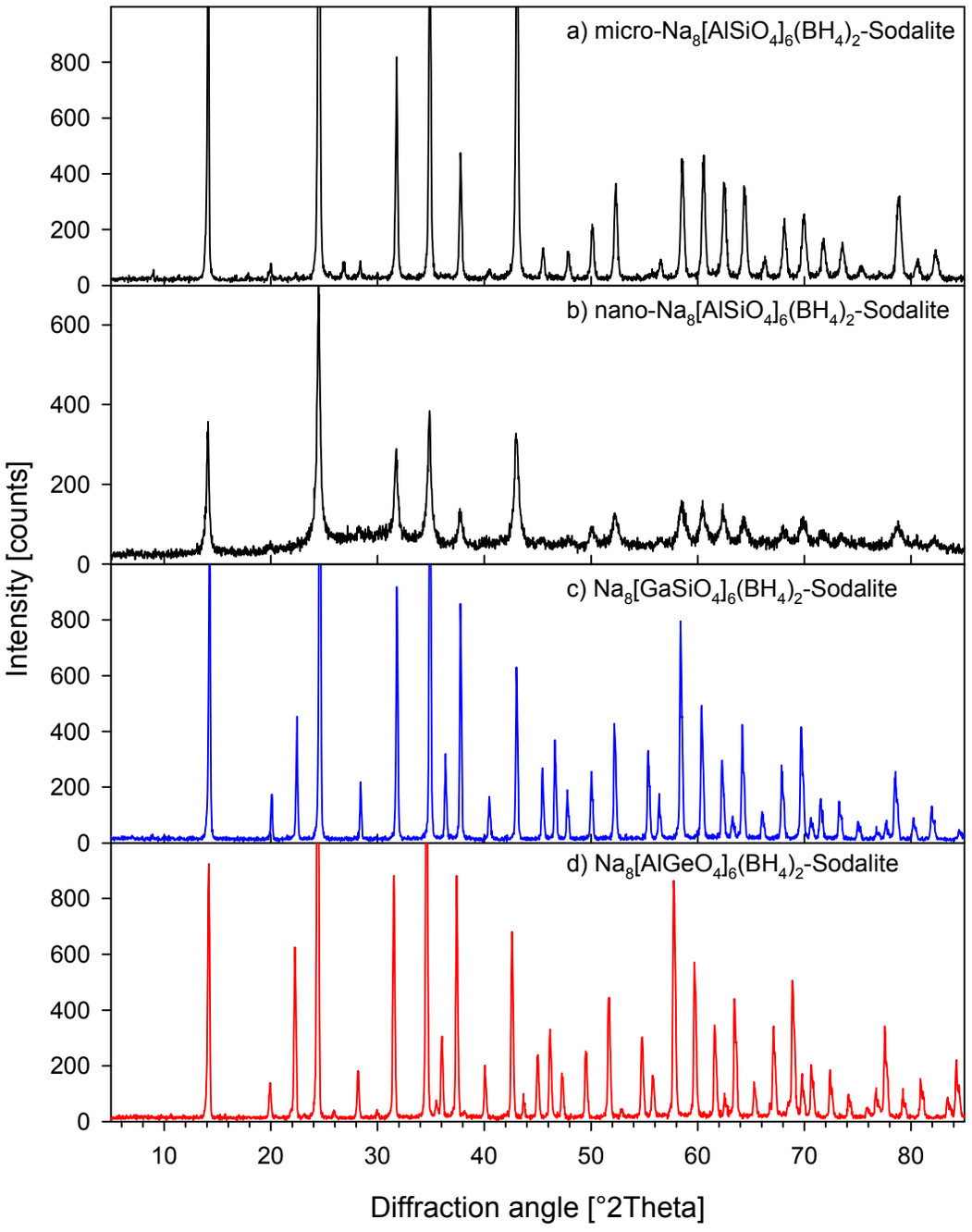

Figure 12. XRD pattern of the $NaBH_4$-sodalites: micro- (a) and nano- (b) crystalline aluminosilicate sodalite, gallosilicate sodalite (c), aluminogermanate sodalite (d).

Formation of crystals of good quality with an average size > 0.5 μm could be stated fom SEM investigations of microcrystalline tetrahydroborate sodalite $Na_8[AlSiO_4]_6(BH_4)_2$ (Fig. 11, left side). For the nanocrystalline sample, obtained after 12 h reaction time (Fig. 11, right side) nanocrystals are "glued together" by amorphous material to larger spherical agglomerates of about 100 nm size [22, 23].

The X-ray powder patterns of the micro- and nano-crystalline aluminosilicate-sodalite, gallosilicate sodalite and aluminogermanate sodalites are shown in Fig. 12. All diffraction peaks of the X-ray powder pattern could uniquely be indexed to pure phase sodalite within P-43n.

Rietveld refinement of the XRD-data for the micro crystalline aluminosilicate sodalite sample showed an amount up to 10 % related to a broad "background contribution" which could be peaked in the range around 30° 2 Theta. This contribution is of importance for hydrogen release from the sodalite as it contains and transports the amount of available water to the sodalite cages as shown below (section 4.1). This contribution which is related to short range ordered sialate type matrix to the sodalite crystals increases in the nanocrystalline sample. This can be seen in Fig. 12 (b) for the nanocrystalline sodalite compared to the XRD pattern of the microcrystalline sample. For this sample, obtained after 12 h reaction time, refinement of lattice constant reveals a = 8.9351(8) Å, being slightly enlarged compared with the microcrystalline phase, a = 8.9161(2) Å. An average crystal size of 25 nm was calculated for this nanocrystalline sodalite and the amount of short range ordered aluminosilicate material could be estimated to about 50 % using the "TOPAS" software [22].

The enclathration of BH_4-anions inside the cages of the micro- and nanocrystalline aluminosilicate sodalite can be seen in the IR-absorption spectra of the samples, Fig. 13. For the microcrystalline sample the aluminosilicate sodalite framework related vibrations, i.e. the six typical peaks can be seen: at about 436 and 469 cm^{-1}; "triplicate peaks" or "sodalite fingerprint" at 668, 705 and 733 cm^{-1} and asymmetric Si-O vibration at 987 cm^{-1} [60]. The BH_4-related vibrations can be seen at 1134 cm^{-1} and the characteristic triplicate peaks at 2240, 2288 and 2389 cm^{-1} by direct inspection in comparison to the spectrum of $NaBH_4$. These peaks are very slightly shifted compared to the peak positions in $NaBH_4$ which could be seen only in an enlarged scale. There are also indications for H_2O contributions around 1630 cm^{-1} (bending of H_2O) and in the range between 3000 and 3600 cm^{-1} (H_2O stretching) related to the water content in the short ranged ordered aluminosilicate. This contribution is significantly enlarged in the nanocrystalline sample. According to this the intensities of the sodalite framework and BH_4^- contribution appear smaller. The IR spectra of gallosilicate and aluminogermanate $NaBH_4$ sodalite are also shown in Fig. 13, too. In both spectra the enclathrated BH_4-anions can be seen by intense absorption bands of the BH_4^- tetrahedral group as compared with the spectrum of the pure salt. The spectrum of the gallosilicate-sodalite framework shows two clear resolved maxima at 922 cm^{-1} and 945 cm^{-1} for the asymmetric T-O-T vibrations. For the ν_s modes two very close adjacent signals with vibrations at 642 cm^{-1} and a shoulder at 624 cm^{-1} as well as a peak at 556 cm^{-1}can be seen from Fig. 13 (c) and finally the framework bending mode was found as one sharp signal at 457 cm^{-1}. The spectrum of the aluminogermanate sodalite Fig. 13 d shows one asymmetric T-O-T mode at 858 cm^{-1}, two symmetric T-O-T vibrations (609 cm^{-1} and 636 cm^{-1}) and a T-O deformation mode at 387 cm^{-1} [18].

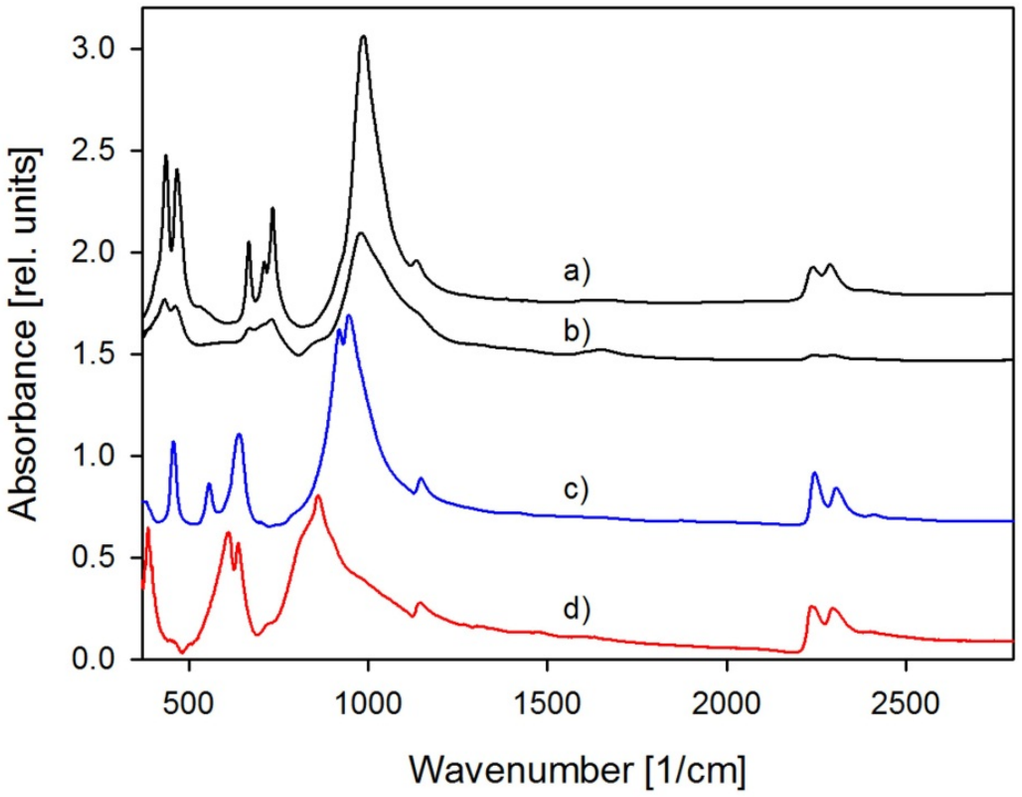

Figure 13. FTIR spectra of $NaBH_4$ aluminosilicate sodalites as synthesized: a) microcrystalline phase, b) nanocrystalline phase and the spectrum of $NaBH_4$ salt (after [22]). Also shown are the spectra of gallosilicate NaBH4-sodalite (c) and aluminogermanate $NaBH_4$-sodalite (d) ([18]).

3.3. Crystal structure of $NaBH_4$ sodalites: X-ray diffraction and MAS NMR study

3.3.1. XRD

The X-ray powder patterns of the microcrystalline aluminosilicate, gallosilicate as well as aluminogermanate $NaBH_4$ sodalites were analyzed by Rietveld method [17]. The atomic parameters of NaCl sodalite were taken as starting values [61] with the BH_4^- group with boron in the centre of the sodalite cage instead of the Cl-anion. Hydrogen was refined on x,x,x positions, restrained to distances of 116.8 pm as found in $NaBD_4$ [62].

The refined positional-, displacement- and occupancy- parameters together with R-values [63], cell constant and cell volume, are collected in Tab. 2 (standard deviation for occupation factors of B and Na: 3%). In the aluminosilicate sodalite the Si-O and Al-O distances are 163(3) pm and 174(3) pm, respectively $l_1 \cdot a$, $l_2 \cdot a$, a = lattice parameter, Fig. 14 a. For example with the formulas as given by [50] some sodalite structure specific parameters as shown in Fig. 3.7 (a) are the tetragonal tetrahedral distortions $\alpha'_{Si} = 112.6°$, $\alpha''_{Si} = 107{,}9°$, $\alpha'_{Al} = 110.8°$, $\alpha''_{Al} = 108.8°$, the tilt angles $\phi_{Si} = 23.7°$ and $\phi_{Al} = 22.3°$, and the Al-O-Si angle $\gamma = 139°$. The "cage filling" configuration could be worked out as illustrated in Fig. 14 b. The Na atoms have three oxygen atoms at 234(2) pm as well as three hydrogen atoms at 267(5) pm in an octahedral arrangement as nearest neighbours. Positional disorder of the hydrogen atoms according to dynamic averaging of orientational disorder is suggested here. Recent ab-initio

calculations could rather closely fit to the experimentally determined structural parameters [64].

$Na_8[AlSiO_4]_6(BH_4)_2$: (SG P-43n: a = 8.9161(2) Å, V = 708.79(2) $Å^3$, R_{WP} = 0.042, R_P = 0.032, R_I = 0.023, R_e = 0.031, d = 0.951)						
Atom	P-4 3 n	occup.	x	y	z	B /10^2nm^3
Na	8e	1.02(3)[1]	0.1834(15)	x	x	2.3(7)
Al	6d	1.0	¼	0	½	1.5(5)[2]
Si	6c	1.0	¼	½	0	1.5[2]
O	24i	1.0	0.1391(28)	0.1487(29)	0.4390(21)	1.1(7)
B	2a	1.1[1]	0	0	0	2.2(34)[3]
H	8e	1.1[1]	0.424(16)	x	x	2.2[3]
$Na_8[GaSiO_4]_6(BH_4)_2$: (SG P-43n: a = 8.9590(1) Å, V = 719.09(3) $Å^3$, R_{WP} = 0.097, R_P = 0.074, R_B = 0.023, R_e = 0.043)						
Na	8e	1.02(2)[1]	0.1731(3)	x	x	2.7(2)
Ga	6d	1.0	¼	0	½	1.1(2)[2]
Si	6c	1.0	¼	½	0	1.1(2)[2]
O	24i	1.0	0.1336(3)	0.1513(3)	0.4310(4)	1.9(2)
B	2a	1.1[1]	0	0	0	3.2(8)[3]
H	8e	1.1[1]	0.4371(38)	x	x	3.2(8)[3]
$Na_8[AlGeO_4]_6(BH_4)_2$: (SG P-43n: a = 9.0589(2) Å, V = 743.40(6) $Å^3$, R_{WP} = 0.112, R_P = 0.082, R_B = 0.026, R_e = 0.043)						
Na	8e	1.02(3)[4]	0.1740(4)	x	x	2.5(2)
Al	6d	1.0	¼	0	½	1.4(2)[5]
Ge	6c	1.0	¼	½	0	1.4(2)[5]
O	24i	1.0	0.1425(4)	0.1441(4)	0.4296(5)	1.6(2)
B	2a	1.1[4]	0	0	0	3.2(8)[6]
H	8e	1.1[4]	0.4401(38)	x	x	3.2(8)[6]

[1-6]Parameters with the same number were constrained to each other

Table 2. Atomic parameters of sodalites $Na_8[AlSiO_4]_6(BH_4)_2$ [17] and $Na_8[GaSiO_4]_6(BH_4)_2$, $Na_8[AlGeO_4]_6(BH_4)_2$ [18]

In the case of gallosilicate sodalite the Ga-O and Si-O distances are 161.1(3) pm and 181.9(3) pm, respectively. The boron atom is located at the centre of the sodalite cage. In a static statistical model of positional disorder the sodium atoms have three oxygen atoms at 234(4) pm as well as three hydrogen atoms at 253(1) pm as nearest neighbours i.e. in principal the same arrangement, as in aluminosilicate sodalite shown in Fig. 14 b. Positional disorder of the hydrogen atoms according to dynamic averaging of orientational disorder is suggested here, too [18]. For the aluminogermanate sodalite the Ge-O and Al-O distances read 173.0(3)

pm and 174.9(3) pm. The sodium atoms in this phase have three oxygen atoms at 234(4) pm and three hydrogen atoms at 257(5) pm as nearest neighbours.

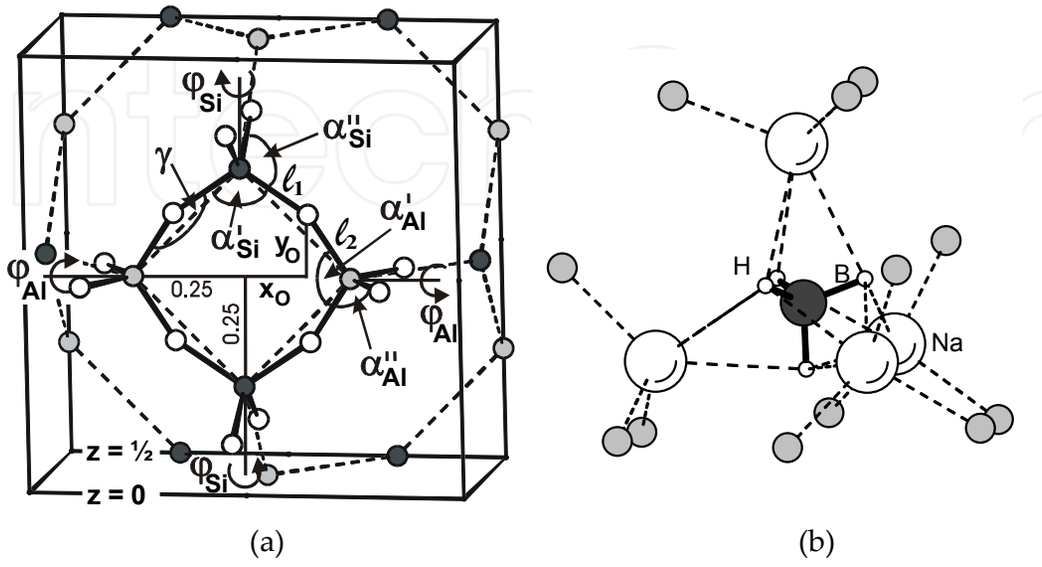

(a) (b)

Figure 14. a, left) Perspective view of one half of the sodalite cage (after [50]) depicting sixring and fourring windows (dashed lines) and denoting bond lengths (l_1, l_2) and tetragonal tetrahedral distortions (α', α''), tilt angles (ϕ) and oxygen coordinates of the framework (x_0, y_0, z_0). Note $z_0 > 0$ determines $\phi > 0$ and z coordinate shifted by ½ compared to values given in Tab. 2. **b, right)** Coordination of the non-framework atoms in the microcrystalline $NaBH_4$ sodalite together with three oxygen atoms of the framework around each sodium atom [17].

3.3.2. MAS NMR

MAS NMR measurements of nuclei the ^1H, ^{11}B and ^{23}Na were performed for the microcrystalline $NaBH_4$ sodalites with aluminosilicate-, gallosilicate- and aluminogermanate framework on a Bruker ASX 400 spectrometer. Further informations on orientational disorder, dynamics and host-guest interaction between framework atoms and BH_4-anions inside the sodalite cages can be derived from MAS NMR spectroscopy [17, 65]. The ^{11}B MAS NMR results of the $NaBH_4$ sodalites are shown in Fig. 15 and in Tab. 2. All spectra were recorded at 128.38 MHz (pulse duration: 0.6 μs; 100 ms pulse delay, 10000 scans were accumulated at a spinning rate of 12 kHz). Chemical shifts were determined using $NaBH_4$ (δ = –42.0 ppm from $BF_3{\cdot}Et_2O$) as an external reference [65]. As a result of boron nitrite of the probehead a broad line is found in all spectra, beside a sharp narrow signal. Thus spectra after subtraction of the broad background are included in Fig. 15. The sharp signals with isotropic chemical shifts (δ_{iso} (^{11}B) around –49.08 ppm (see Tab. 3) are typical for boron tetrahedrally coordinated by four hydrogen atoms [66]. The full-width at half-maximum (FWHM) of the sharp lines are included in Tab. 3.

^{11}B MAS NMR				
Sodalite	δ_{iso} [ppm]	FWHM [ppm]	C_Q [kHz]	η_Q
AlSi	–49.08	1.70	–	–
GaSi	–49.91	1.28	–	–
AlGe	–49.01	1.11	–	–
^{23}Na MAS NMR				
AlSi	–6.61	4.43	8.82	0
GaSi	–1.31	2.32	6.41	0
AlGe	–1.60	1.88	6.75	0.22

Table 3. Isotropic chemical shift (δ_{iso}), quadrupolar coupling constant (C_Q), asymmetry parameter (η_Q), Lorentzian/Gaussian broadening (FWHM) of the ^{11}B MAS NMR spectra of $NaBH_4$ aluminosilicate (AlSi), gallosilicate (GaSi), aluminogermanate (AlGe) sodalite [65].

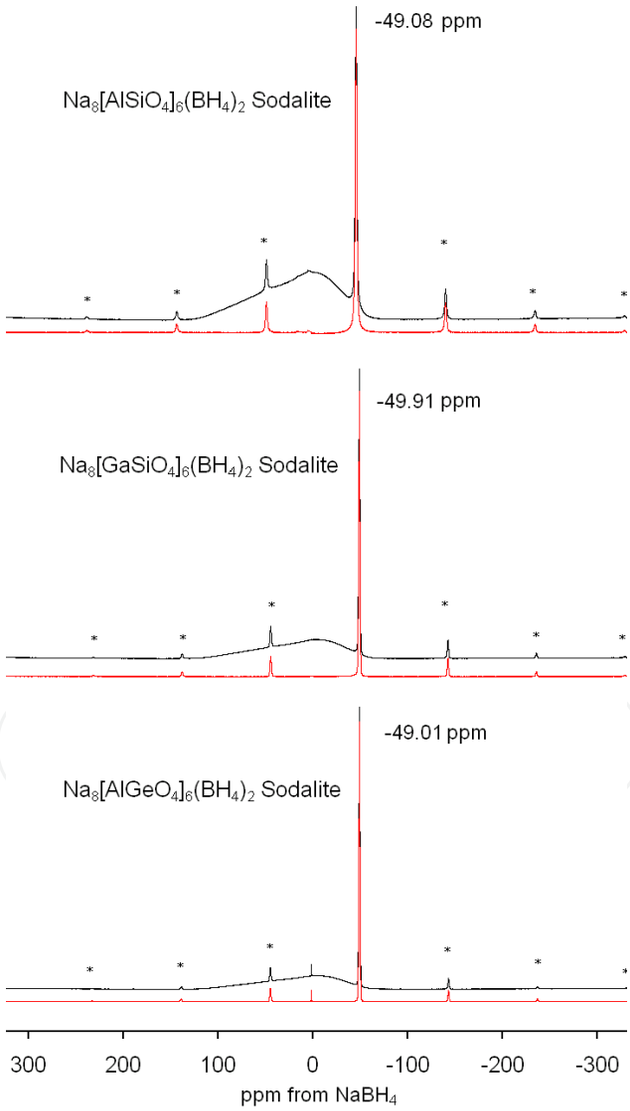

Figure 15. ^{11}B MAS NMR spectra of the microcrystalline $NaBH_4$ sodalites; asterisks mark the spinning side bands, lower spectra are given after the subtraction of the probe background (after [65]).

Compared with pure $NaBH_4$ ($\delta^{11}B$ = -42.0 ppm) a slight downfield shift of the signals can be found for all three sodalites as a result of the matrix effect of the surrounding framework atoms. The nearly equal values of the chemical shifts for the three sodalites indicate no significant influence of framework composition on the arrangement or the shape of the BH_4-anions inside the sodalite cages [65]. Threefold-coordinated non-framework boron or four-coordinated framework boron can also be excluded from the distinct chemical shift values of the sharp signal in all three cases, because ^{11}B of BO_3-units resonates in the range between 12 and 25 ppm, and BO_4-groups exhibit these shifts in the approximate range between –4 ppm and –6 ppm [66, 67].

Following [65] further informations can be derived from the signals. The sharp and narrow lineshape of the signals show almost no quadrupolar interactions due to the discreet BH_4-unit possessing a highly symmetrical environment for boron in the sodalite-cage as well as possibly fast dynamic site exchange of hydrogen. Because of a relatively low C_Q (~ 0.501 MHz) value expected for BO_4-groups, and a larger value (C_Q ~ 2.5 MHz) expected for BO_3-units [66-68] the present quadrupole coupling parameters rule out any contribution of BO_3- or BO_4-units. A small contribution at +2 ppm can be seen in the spectrum of aluminosilicate sodalite after subtracting of the probehead signal. This signal could be attributed to a small amount of $B(OH)_4$-anions in the sodalite cages. A similar signal at about 1.7 ppm is known in the ^{11}B MAS NMR spectrum of $NaB(OH)_4$-aluminosilicate sodalite [69].

The ^{23}Na MAS NMR signals were recorded at 105.84 MHz (pulse duration: 0.6 μs, pulse delay: 100 ms; accumulation of 5000 scans; spinning rate: 12 kHz; external reference: solid NaCl salt). The "dmfit2003" software was used for peak fitting [70]. The ^{23}Na MAS NMR spectra are given in Fig. 16 (left). Further informations on chemical shifts, FWHM and quadropolar parameters C_Q (quadrupole coupling constant) and η_Q (asymmetry parameter) are summarized in Tab. 3. The signals exhibit a narrow line shape typical for a single type of sodium coordination indicating nearly no quadrupole interactions according to the very small quadrupole parameters (C_Q and η_Q in Tab. 3). This implies well defined position probably caused by highly symmetric and cubic orientation of the BH_4-anions on the one side and the framework oxygen on the other side but also enables dynamic fast motion of the guest atoms within each sodalite cage leading to motional narrowing.

The ^1H MAS NMR spectra were obtained at 400.13 MHz with a single pulse sequence duration of 1.5 μs (90 degree pulse length of 6.5 μs) and a recycle delay of 5-30 s. 100 scans were accumulated with a spinning rate of 14 kHz, and tetramethylsilane (TMS) was used as an external reference. The high spinning speed helps to remove any residual dipolar broadenings. The ^1H MAS NMR spectra of the sodalites, given in Fig. 16 (right) exhibit a single sharp intense line at a chemical shift of about –0.6 ppm for all three sodalites assigned to the hydrogen atoms of the BH_4-groups. This indicates that proton chemical shift is not influenced by the chemical composition of the sodalite framework. A shift in high field direction, compared with $NaBH_4$ salt ($\delta(^1H) \approx 1.0$ ppm) results from the enclathration of single BH_4-groups in contrast to their incorporation in the NaCl-type structure of the salt and its strong heterovalent bonds [65]. A further but weak signal at ~ 5.0 ppm in each spectrum could be related to water molecules enclathrated in distorted sodalite cages [71] or

following the interpretation due to water incorporation in short range ordered sialate bonds. The nature of the shoulder of the main signal at about 0.6 ppm could be related to enclathrated water molecules or to $B(OH)_4$-impurities as observed in ^{11}B NMR signals, too. A third less intense signal at 1.2 ppm appears only in the spectrum of the aluminogermanate sodalite. It could indicate small amounts of ($H_3O_2^-$)-impurities in a few sodalite cages [71, 65].

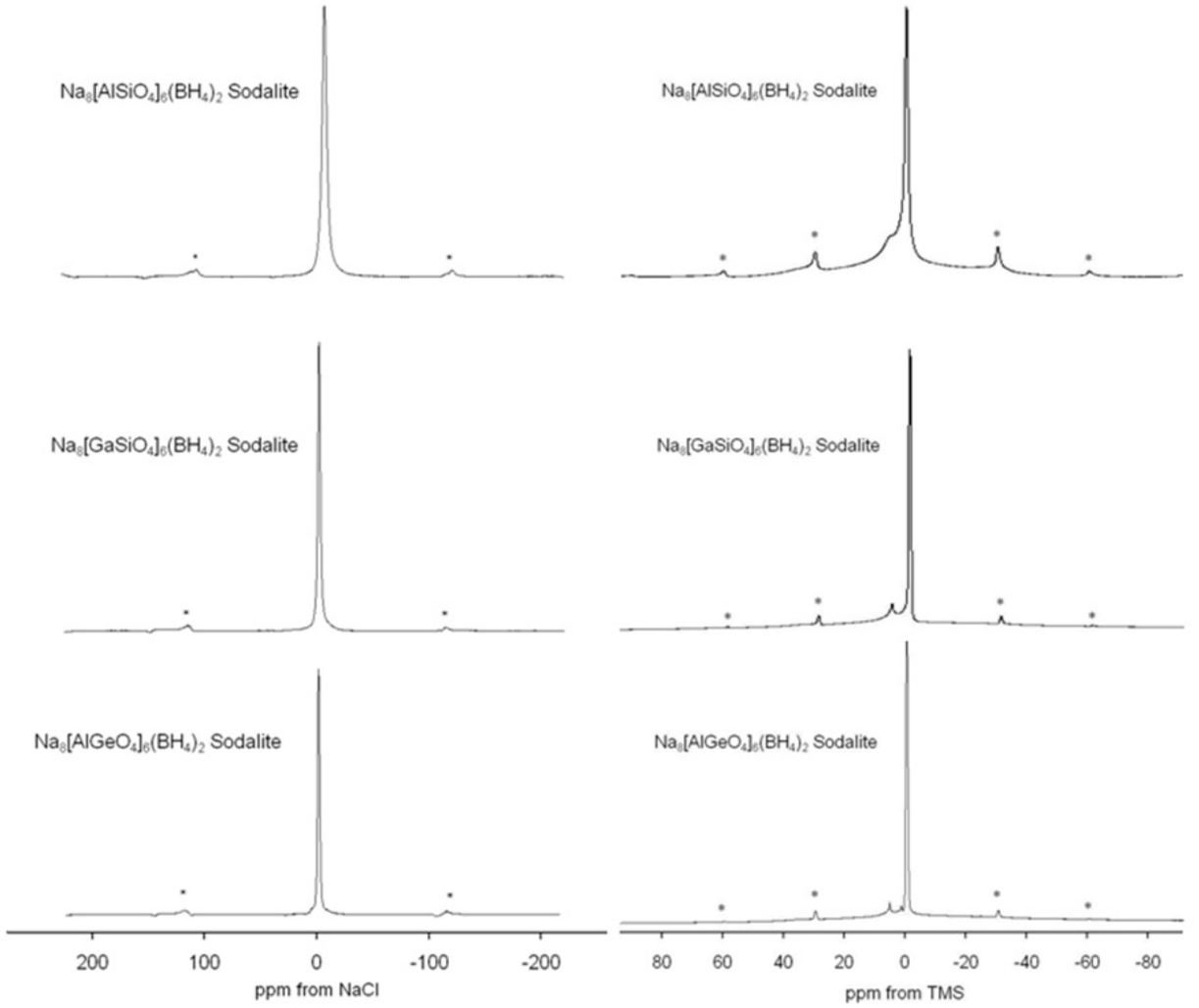

Figure 16. (left) ^{23}Na MAS NMR spectra of the microcrystalline $NaBH_4$ sodalites; asterisks mark the spinning side bands (after [65]). **Fig. 16 (right)** ^{1}H MAS NMR spectra of the microcrystalline $NaBH_4$ sodalites; asterisks mark the spinning side bands (after [65]).

4. Hydrogen release and reinsertion experiments with the BH_4-sodalite samples

This section shows that the BH_4-anion enclosed in the sodalite cage enables a controlled release of hydrogen with water in consecutive steps when heated (4.1). Experiments of regeneration of the pre-reacted BH_4-anion in the sodalite cage are presented (4.2). A basic understanding could be achieved using temperature dependent infrared (TIR) absorption experiments [38]. Since this method is used intensively in this chapter it may be described here briefly. In TIR

experiments typically around 1 mg of sample are diluted in 200 mg NaCl or KBr powders and pressed into pellets. The pellets are fixed in an Ag tube (Fig. 17) which can be heated in a furnace to the desired temperature. In this arrangement transmitted IR light (I) can be monitored in situ as absorbance = $-\lg(I/I_0)$, where I_0 is the transmitted intensity through a reference pellet. The measurements were conducted under vacuum in an appropriate IR sample chamber (FTIR Bruker IFS 66v) to avoid disturbances by variations in the outer atmosphere during the measurements. With increasing temperature dehydration effects of the matrix (KBr, NaCl) could occur if not dried sufficiently before its use. As shown below, additives to the matrix as for example the addition of KNO_3, could be used in order to tracer the effect of hydrogen release by reduction. Thermogravimetric (TG) and differential thermal analytical (DTA) measurements were carried out using a commercial instrument (Setaram Setsys evolution 1650). Flowing atmospheric conditions of various gases were used with the sample carried in corundum crucibles. Further hydrogen reloading experiments were performed with controlled hydrogen pressures up to 200 bars and temperatures up to 400°C using in house built autoclaves with equipment as shown in Fig. 18. The pressure was checked permanently during heating by the manometer. For the experiments the samples were filled into Au capsules which were only closed by slightly pressing the ends together for realizing a throughput for gas. Temperature calibrations of the autoclave were carried out between 100 and 400°C obtaining a precision within 5°C for the absolute value. The heating rate was 4°C/min. After the chosen holding time at a fixed temperature, the autoclave was cooled down rapidly, e.g in 10 minutes from 300°C.

Figure 17. Ag tube, a pressed pellet (diameter 13 mm), and two silver nets for supporting the pellet in the tube and improve the thermal contact during the temperature dependent infrared (TIR) measurements.

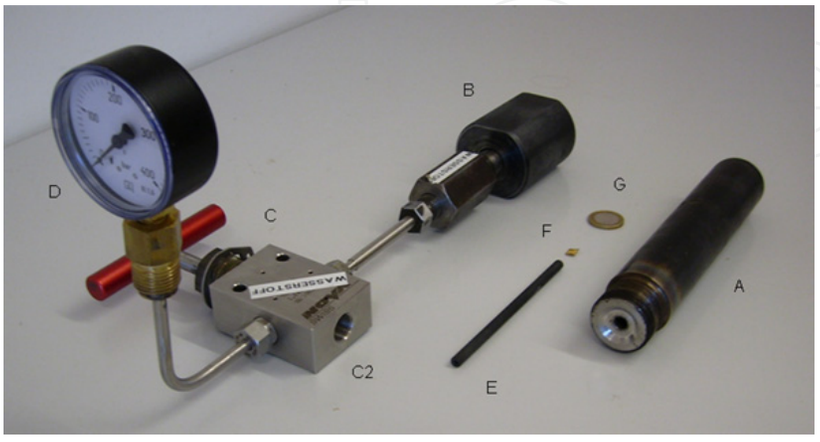

Figure 18. Equipment for hydrogen pressure experiments: Autoclave (A), connection piece (B) between autoclave and closing device with three-way switch (C) with opening to the outer hydrogen bottle (C2) and to the manometer (D). Filling piece (E) and Au capsule (F).

4.1. Variation of cage anions of $Na_8(AlSiO_4)_6(BH_4)_2$ when heated

The effect of various heating rates and heating temperatures in ex situ TG experiments as well as in situ TIR measurements in dry and wet NaCl environments has been investigated for the microcrystalline $NaBH_4$-sodalite. Heating with a constant rate of 2°C/min to 300, 400 and 500°C (He-flowing conditions, 20 ml/min) reveals weight losses of about 0.2 %, 0.6 % and 0.9 %. This weight loss is related to dehydration and to hydrogen release. The dehydration corresponds obviously to water contained in some short range ordered sialate bonds as explained in section 3.2 (compare also below peaks denote HOH and D in Fig. 19). In experiments with heating rates of 2°C/min, 4°C/min and 6°C/min to 300°C the weight loss reads 0.2 %, 0.4 % and 0.7 %, respectively. Thereby the IR absorption intensity of BH_4 related peaks decreases about 11 % at heating rate 2°C and 7 % at heating rate 6°C/min. This shows that the faster the heating rate the lesser the loss of BH_4-anion in the sodalite cage. Therefore, the faster the heating rate the more water leaves the sample without use for hydrogen release and, accordingly, the higher the weight loss. The spectra of the samples taken after cooled down to room temperature (rate 2°C/min) from 300, 400 and 500°C, exposed to atmospheric conditions and pressed into KBr pellets are shown in Fig. 19. Compared to the unheated sample the BH_4 related intensity has decreased by about 15.5 %, 13 % and 11 % when heated to 500, 400 and 300°C, respectively. Related with the decrease in BH_4-anion concentration new peaks appear denoted in the spectra by A, B, B′ and C. This notation follows that given earlier [17, 22] relating peak A, B, B′ to anions H_3BOH^-, $H_2B(OH)_2^-$ and $HB(OH)_3^-$, respectively. According to this the following reactions could be seen:

$$H_4B^- + H_2O = H_3B(OH)^- + H_2;\ \text{peaks A } (A1,\ A2) \tag{1}$$

$$H_3B(OH)^- + H_2O = H_2B(OH)_2^- + H_2\ ;\ \text{peak B} \tag{2}$$

$$H_2B(OH)_2^- + H_2O = HB(OH)_3^- + H_2\ ;\ \text{peak B'} \tag{3}$$

A further reaction of hydrogen release followed by two steps of dehydration which finally leads to peaks C could be suggested as:

$$HB(OH)_3^- + H_2O = B(OH)_4^- + H_2 \tag{4}$$

$$B(OH)_4^- = BO(OH)_2^- + H_2O \tag{5}$$

$$BO(OH)_2^- = BO_2^- + H_2O\ ;\text{peaks C} \tag{6}$$

The step eq. 4 which reveals the anion species $B(OH)_4^-$ is not seen directly due to fast dehydration above about 400°C as known for the $B(OH)_4$-sodalite [72, 38]. For better comparison appropriate spectra of microcrystalline $Na_8(AlSiO_4)_6(B(OH)_4)_2$ and those obtained

by dehydration at 200°C for $Na_8(AlSiO_4)_6(BO(OH)_2)_2$ and at 400°C for $Na_8(AlSiO_4)_6(BO_2)_2$ are shown in Fig. 20. The BO_2-anion in the sodalite cages can markedly be observed by means of the peaks at about 1958 and 2029 cm^{-1} denoted as peaks C here. The anion species $BO(OH)_2^-$ shows characteristic peaks in the range 1490-1520 cm^{-1} (denoted C′ further below) and around 1150 cm^{-1}, beside the OH-stretching at about 3610-3620 cm^{-1} compared to the OH-stretching of the $B(OH)_4$-anion at 3620-3640 cm^{-1} [38]. According to this BO_2-anion species in Fig. 19 can readily be identified indicating that reactions eq. 4, 5 and 6 occurred.

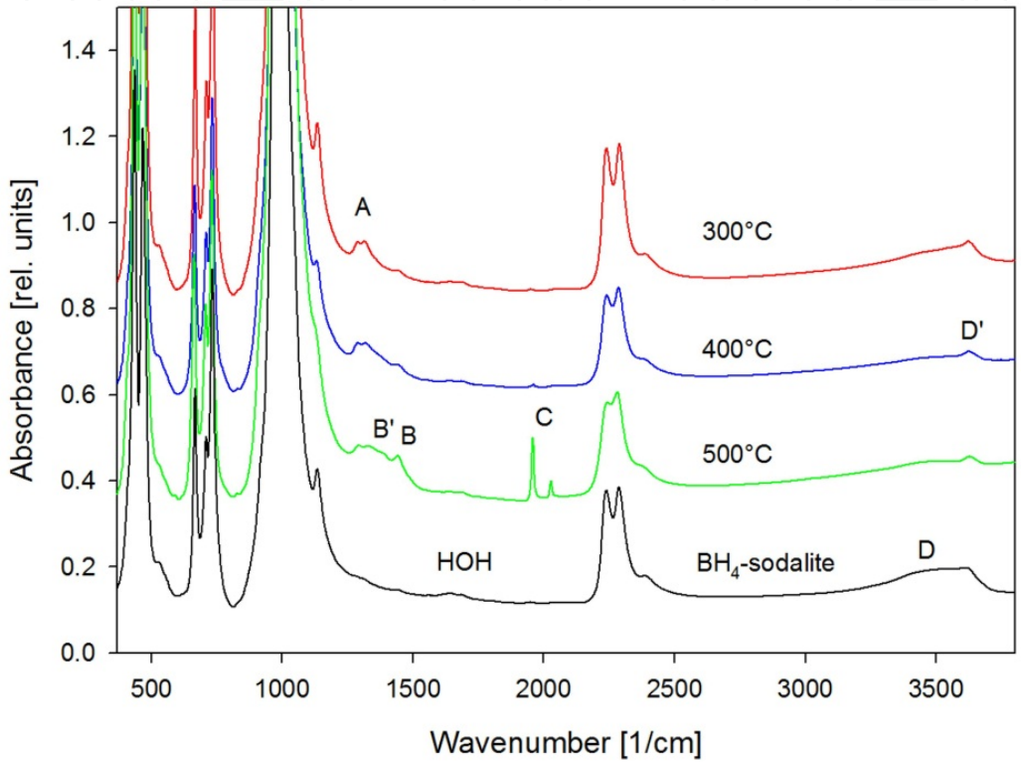

Figure 19. IR-absorption of BH_4-sodalite before and after heated to 300, 400 and 500°C. For peaks denoted A, B, B′, C, D, D′ and HOH see text.

The microcrystalline sodalite shows a sharper peak which remains present during heating (see below) with maximum at about 3620 cm^{-1} denoted as D′. As discussed by [17, 22] D′ could be related to an OH-anion in the sodalite, indicating basic or hydro-hydroxo sodalite. D′ could also be related to the formation of B-OH forms or to superimposition effects of various species. A clear distinction is hard to obtain. Another important contribution is the presence of water molecules indicated by H-O-H bending vibrations at about 1640 cm^{-1} and OH stretching at 3000-3600 cm^{-1} called D in Fig. 19. It could be observed that these contribution becomes partly dehydrated during heating and are in some extend related to the hydrogen release reactions. If the sample is dehydrated the hydrogen release reaction invariably stops. It could be shown that all the sodalite with all formed species remains stable below 600°C also at invariably long time. Heating above 630°C immediately leads to framework destruction. These thermal instabilities were investigated in detail by [19, 20].

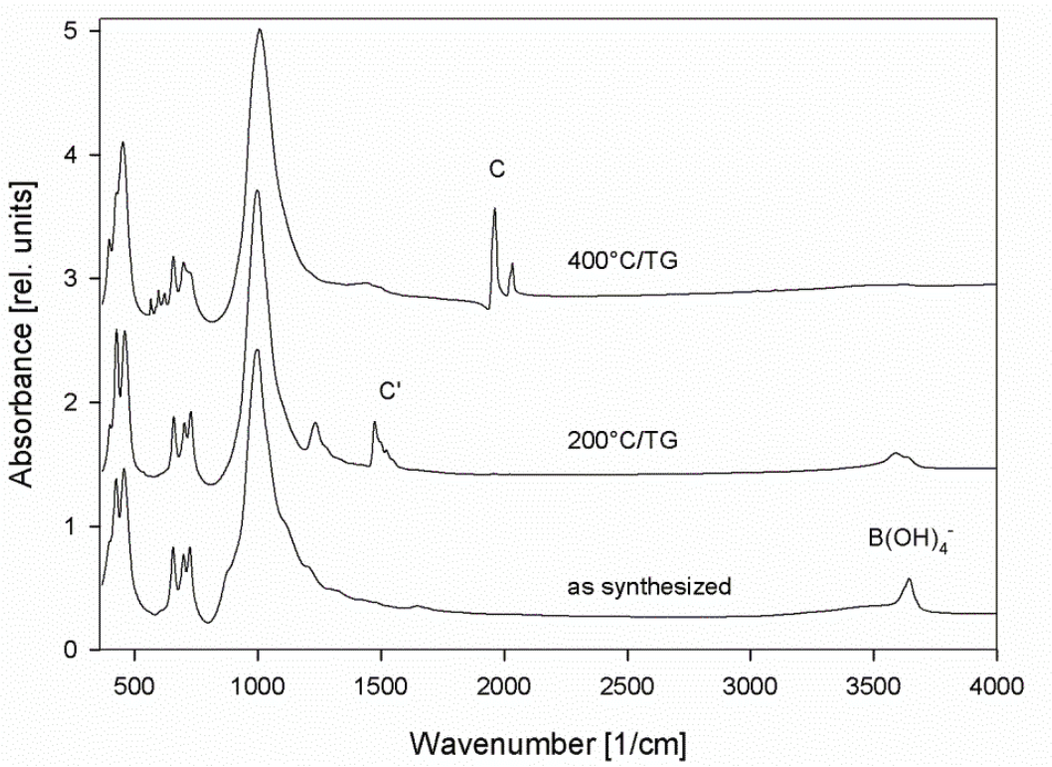

Figure 20. IR-absorption of $B(OH)_4$- sodalite (as synthesized), after dehydration at 200°C to $BO(OH)_2$-sodalite and at 400°C to BO_2- sodalite.

The effect of rehydration could be used to further proceed the hydrogen release reactions as shown in Fig. 21. The sample preheated at 500°C was taken out of the thermobalance, exposed to atmospheric conditions and run again up to 500°C under He conditions in 7 further cycles. Spectra obtained after each run show a gradual decrease of BH_4-absorption intensity and increase in BO_2^- content (Fig. 21). Similar to the C peaks, the B peak also becomes a bit more pronounced, whereas the peaks B' and A become broader and more unspecific. The framework vibrations remain largely unchanged and may depict only the changes due to the changed borate species, i.e no significant destruction of the framework is observed. Thus these experiments show the high stability of the sodalite during several heating cooling cycles. A certain amount of water content related to the matrix consisting of short range ordered sialate bonds of the sample is reloadable and can be used to continue the hydrogen release reactions. An exponential decay of the ratio BO_2^-/BH_4^- could be observed (inset in Fig. 21). There is a significant increase in intensity in the range of peak B above about 400°C, too. There is further work to do to find out whether here intracage reactions occur or if borate species outside the sodalite cages are formed which could be related with a destruction of the framework. Explanation could, however, also be given with an other anion in the cage, e.g. H_2BO^- (compare below, eq. 7, 8).

The reaction sequence of hydrogen release may be followed in more detail for the microcrystalline $NaBH_4$-sodalite in TIR experiments as shown in Fig. 22. In the lower part spectra are shown when cooled down to room temperature after heating to 200, 300, 400 and 500°C in NaCl pressed pellet. In the upper part the spectra are taken at denoted temperatures. It can be seen that peaks A grow in intensity followed by B and B' with

increasing temperature. The formation of $B(OH)_4$-anions may not be detected as they become dehydrated to $BO(OH)_2$-anions as indicated by peak C′ at temperatures between 250 and 450°C. Above this temperature the formation of BO_2-anions is indicated by the peaks C (C1, C2). In TIR experiments of the 500°C pre-reacted sample it was observed that the C peak intensitity (BO_2^-) decreases from about 200°C and increases again in intensity above about 370°C. Complementary to this the intensity related to ($BO(OH)_2^-$) (called C′, Fig. 22, right) increases and decreases. Additionally the BH_4^- intensity decreases above about 370°C. This indicates that in a first step the reacting water must rehydrate the BO_2^- species and finally effectively reaches the BH_4-anions in the centre of the sodalite crystals. This implies that the reactions are controlled by the diffusion through the sodalite cages. The diffusing species might mainly be OH^- and H^- via defect formation in the cages. Thus water disproportion and H_2 formation may occur at the crystal surface.

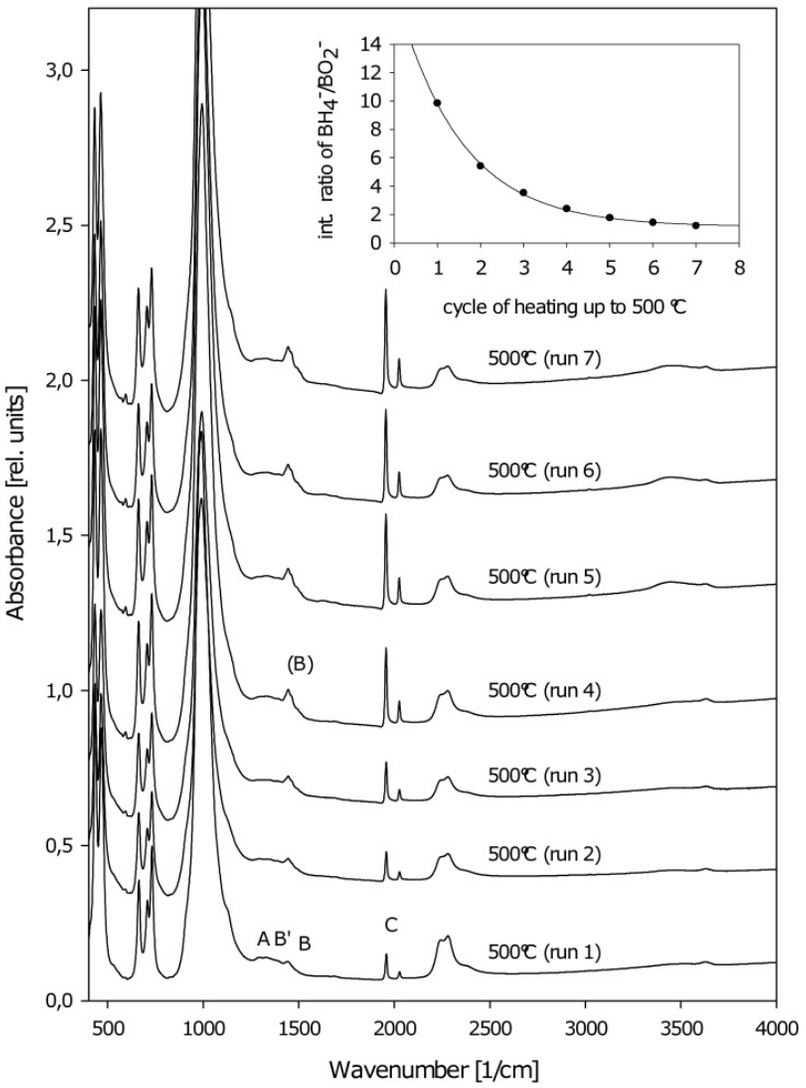

Figure 21. IR-absorption spectra of BH_4-sodalite sample of nominal composition $Na_8(AlSiO_4)_6(BH_4)_2$ (as synthesized) after thermal treatment at 500°C (heating rate 2°C/min, 0.5 h holding time, flowing He 20 ml/min). Spectra were taken after each cycle and exposure the sample to atmospheric conditions for 24 h by KBr method for a part of the sample. The remaining sample was given to the next thermal treatment.

A closer view of the characteristic sodalite fingerprint peaks ν_1, ν_2, ν_3 is shown in Fig. 22 (left). A significant shift of ν_1, ν_2, ν_3 towards lower wavenumbers occurs with increasing temperature which is almost completely reversible with decreasing temperature (Fig. 23). The small deviations can be related to the changes in the cage filling species. TIR experiments were also carried out using KBr pressed pellets to demonstrate the effect of an exchange of Na-cations from the sodalite with K-cations from the matrix as indicated by the strong deviation in temperature dependance of ν_1, ν_2, ν_3 from the effect observed using NaCl pellets (Fig. 23). A significant exchange occurs above about 250°C which could be similarly demonstrated for other sodalites, too [38]. This indicates that the Na-cations become highly mobile as could also be observed in temperature dependent investigations using MAS NMR [73] and XRD structure refinements [50] on related sodalite compositions. It can be concluded that above 250°C the jump rate of Na^+ in the cage and through the sixring windows becomes very significant which implies that the out-in jump rates of other ions could also increase.

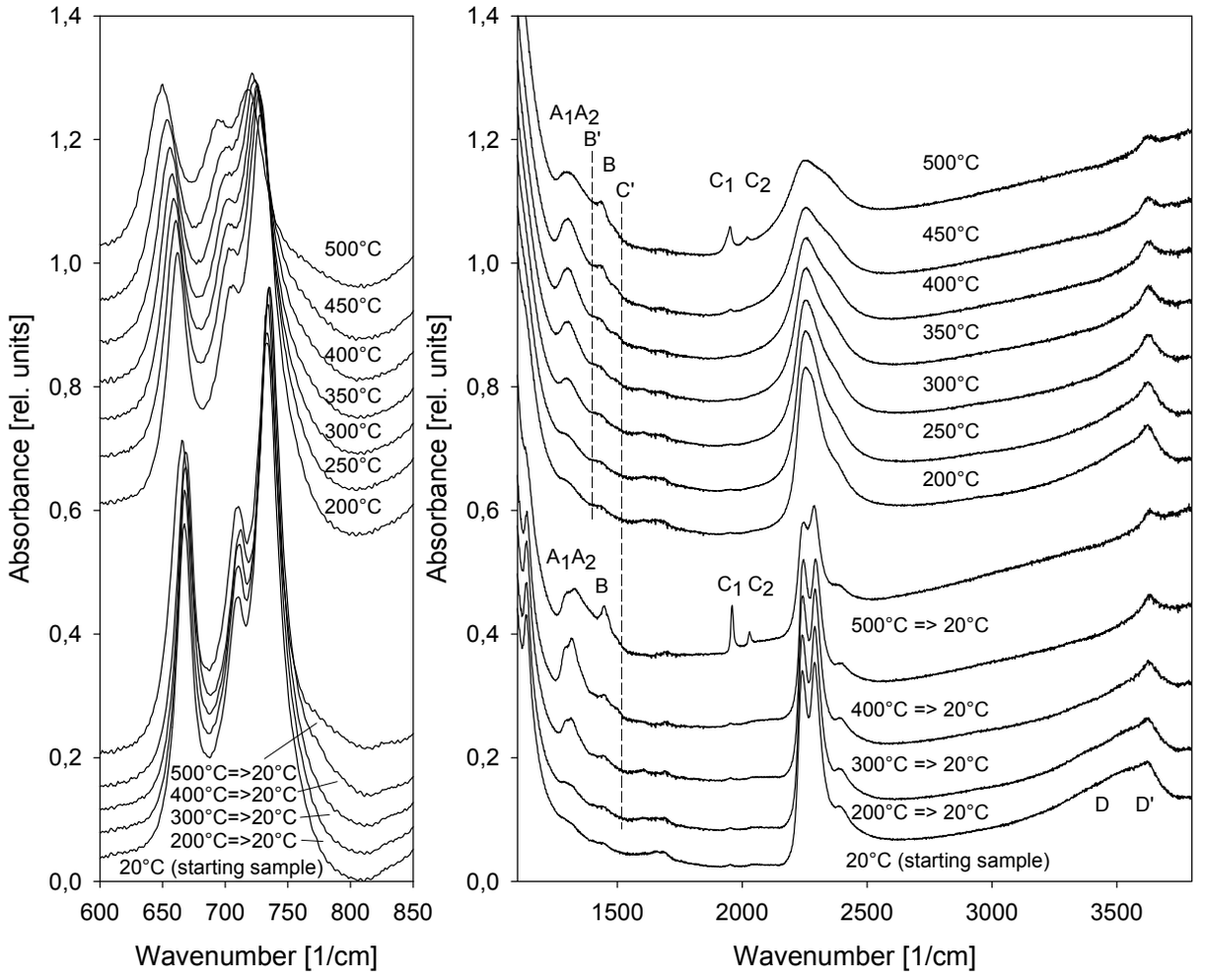

Figure 22. TIR absorption spectra of BH_4-sodalite sample of nominal composition $Na_8(AlSiO_4)_6(BH_4)_2$ (as synthesized) of the starting sample at 20°C and taken in the heating up run at temperatures as denoted (upper part) and at 20°C when cooled down from temperatures as denoted (lower part) for the range of the characteristic sodalite fingerprint of framework vibrations ν_1, ν_2, ν_3. (left) and the cage filling species (right).

The change in peak intensities obtained in the NaCl related TIR experiment (Fig. 22) for peaks A, B, C′ and C could be evaluated in more detail as shown in Fig. 24. The intensity of A peaks increases significantly above about 220°C, crossing over in an effective temperature independent behaviour above about 320°C. About at that temperature peak B and also C′ start to increase in intensity. The later effect shows that dehydration occurs as described by eq. 5. This implies that reaction eq. 4 occurred rather fast which could not be resolved. Species B′, i.e. eq. 3, could not be considered separately because of superposition in the spectra with peaks A and peak B. A decrease in intensity of peaks A, C′ and also B′ is observed above about 450°C where peaks C start to increase strongly in intensity. This shows that above 450°C strong dehydration occurs leading finally to the BO_2-anion in the sodalite cage. It can be suggested that part of this water is used for a further effective hydrogen release with reactions as given by eqs. 1-4.

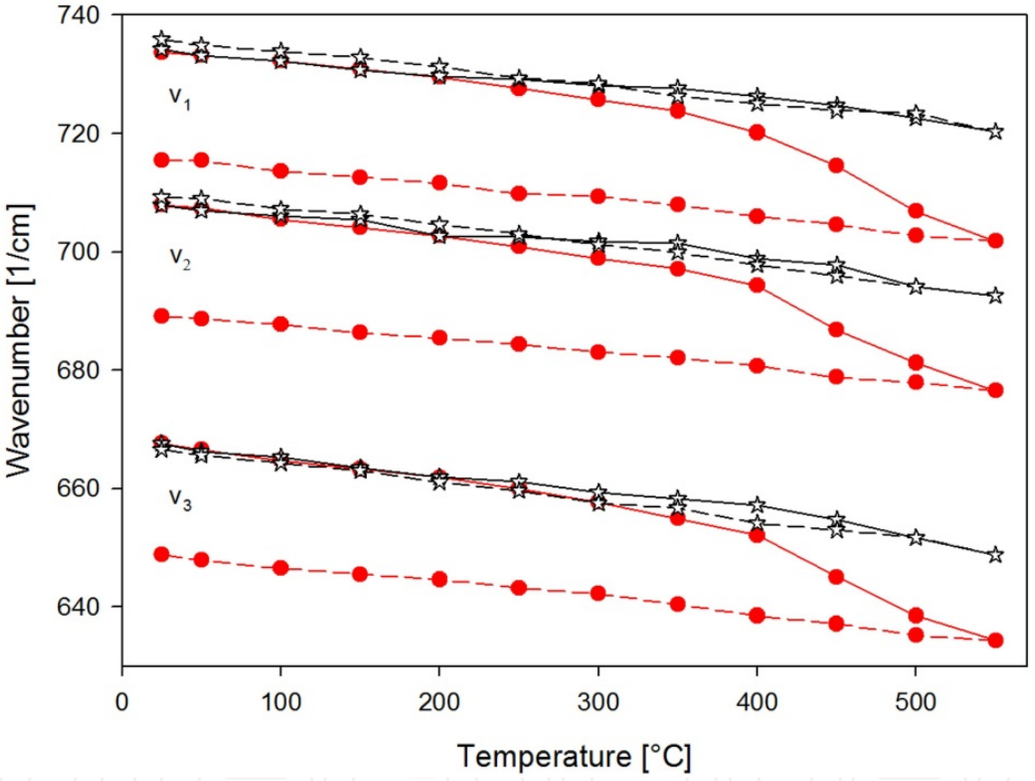

Figure 23. Temperature dependence of framework peaks ν_1, ν_2, ν_3 when heated in NaCl pellet (open stars) and in KBr pellet (closed circles) taken in the heating up run (connected by thin solid line) and when cooled down (connected by dashed line).

One interesting point is that the peak intensity of peak B also re-increases above about 450°C. If this effect is related to further hydrogen release reaction or to a dehydration reaction or a dry hydrogen release of the type eq. 7 or 8 [17, 22] requires further investigations.

$$HB(OH)_3^- = H_2BO^- + H_2 \tag{7}$$

$$H_2B(OH)_2^- = H_2BO^- + H_2O \tag{8}$$

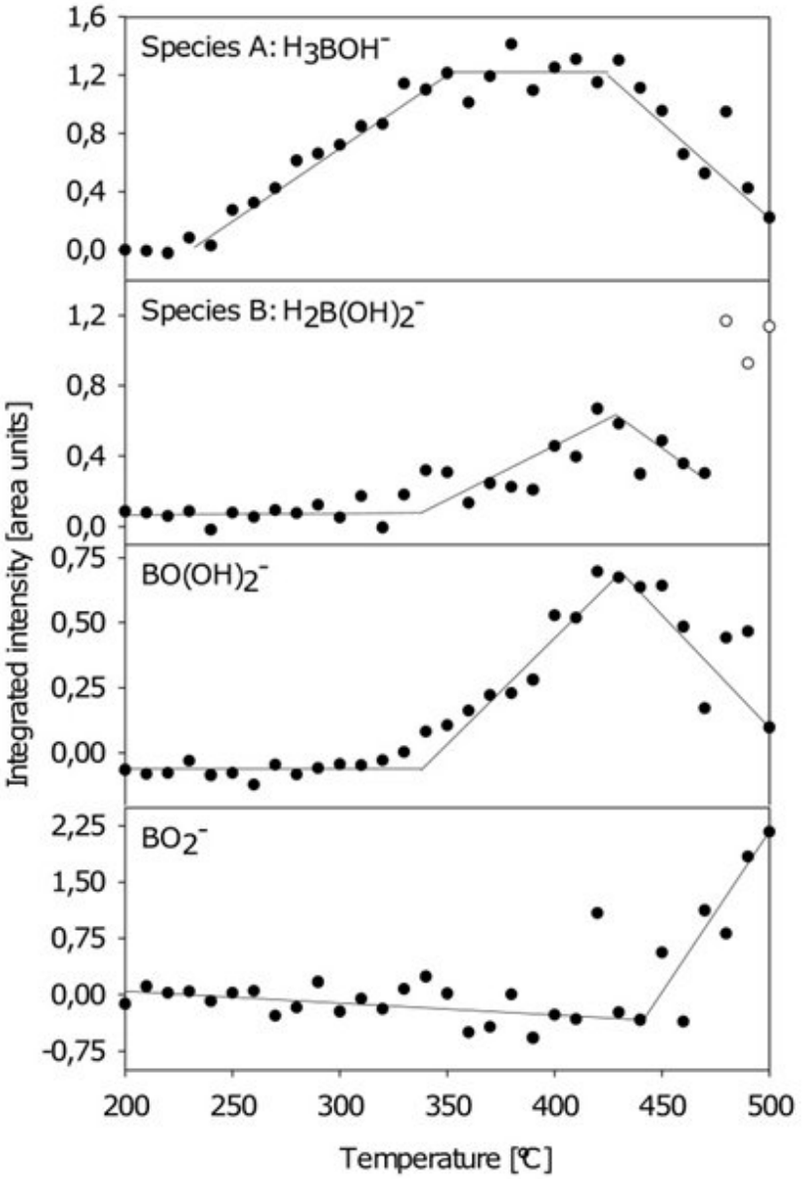

Figure 24. Temperature dependence of intensities of characteristic peaks of intra cage anion species as denoted. Thin solid lines are guide to the eyes. Open circles in the species B panel mark the re-increase of intensity when heated above 475 °C (compare text).

A proof that hydrogen is released is given using a nitrate tracer reaction in TIR experiments [22, 24, 74] as shown in Fig. 25. Here some amount of KNO_3 has been added to the sample pellet which could be identified as an additional peak in the spectra (see inset in Fig. 25). With increasing temperature this peak strongly decreases in intensity above about 250°C. Repeating the TIR experiment with only KNO_3, it shows a slight decrease in intensity of the KNO_3 related peak above about 400°C due to a gradual thermal decomposition. Therefore, it can be concluded that hydrogen is released from the BH_4-sodalite sample leading to a redox reaction with KNO_3. Since this reaction cannot be achieved by hydrogen molecules (compare below, Fig. 27) it can also be concluded that hydrogen is set free in an activated form.

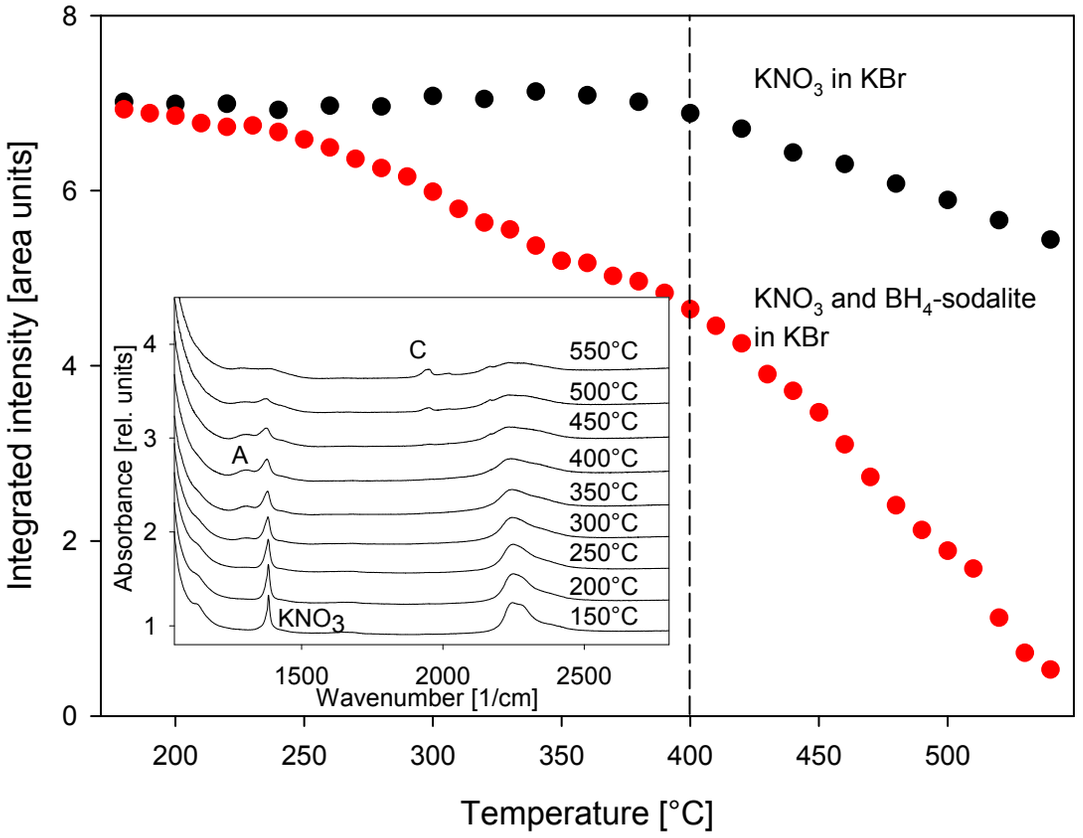

Figure 25. TIR experiment with the addition of KNO_3. Main figure shows the temperature dependence of the integrated intensity of the KNO_3 related peak in the pellet with the BH_4-sodalite (compare spectra given in the inset) compared to the behavior observed without. Dashed vertical line marks temperature of decomposition known for KNO_3.

Another interesting point is the effect of using "wet NaCl" for the pressed pellet in the TIR experiment as this increases the amount of H_2O available for the hydrogen release reaction from the embedded BH_4-sodalite. This even leads to a complete decrease of the BH_4-content with increasing temperature. The loss in BH_4-intensity in "dry NaCl" and "wet NaCl" are compared in Fig. 26 demonstrating again the effect of the different amounts of available H_2O content for the hydrogen release reaction. Included is the observed effect for nanocrystalline BH_4-sodalite as well, also using dry NaCl and wet NaCl. Here the difference is marginal distinct since the nanocrystalline sample contains a much higher amount of water related to the higher contribution of short range ordered sialate bonds. Moreover the reaction path for hydrogen release is found at significantly reduced temperature due to the much smaller crystal size.

4.2. Experiments on regeneration of pre-reacted BH_4-sodalite

Based on the observation that the hydrogen release reactions of the BH_4-anion in the sodalite cage with H_2O could be carried out in consecutive steps it seems likely that all reactions according to eqs. 1-4 or at least some are reversible. It can be concluded that hydrogen release from BH_4-sodalite crystals is a diffusion controlled process were OH-anions

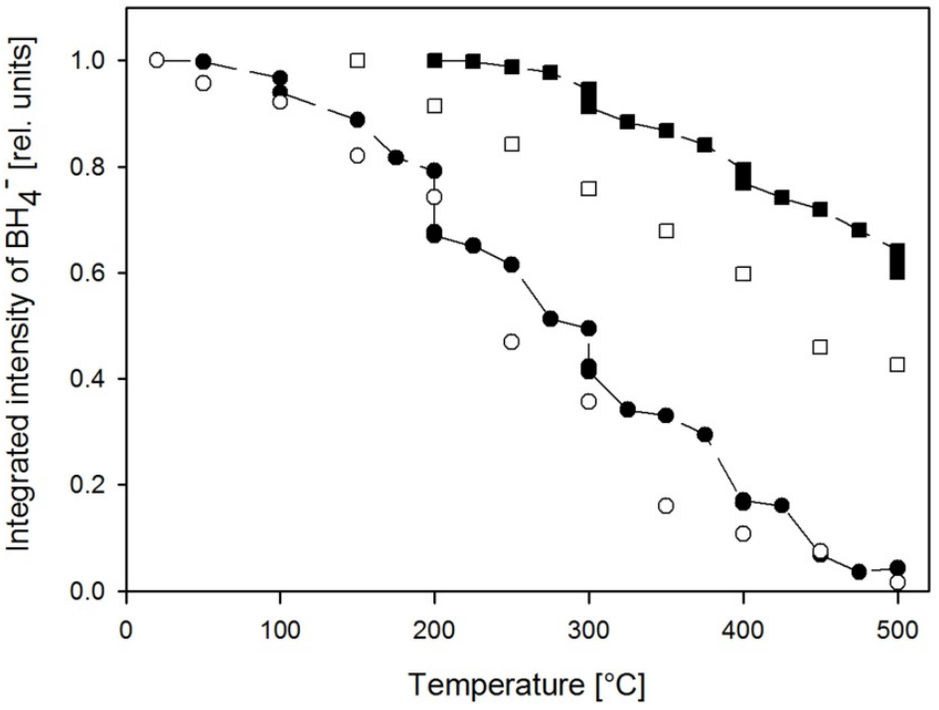

Figure 26. Integrated intensity of the BH_4-anion absorption. Closed and open squares for micro BH_4-sodalite in dry and wet NaCl, respectively. Closed and open diamons for nano BH_4-sodalite in dry and wet NaCl.

diffuse inward and H-anions outward. Following this, the reinsertion reaction seems only be possible if appropriate H^-/OH^- gradients could be realized which should govern the efficiency of "reactor regeneration". This assumption could be supported by the "nitrate reduction reaction" observed in Fig. 25. Following reference [75] such type of low temperature nitrate reduction can not be achieved by hydrogen molecules. It has been shown that hydrogen molecules need to be activated by the presence of special catalysts, e.g. Pt or Pd. This requirement could be demonstrated in TG/DTA experiments with heating/cooling runs with as received commercial KNO_3 (Merck) with and without the addition of Pt powder (Fig. 27). Using pure KNO_3 the effect of the structural phase transition can be seen at 140°C and 130°C in the heating up (20°C/min) and cooling down (20°C/min) run as endothermic and exothermic peak, respectively. There is a negligible weight loss of less than 0.5 %, which could be related to dehydration effect. The experiments were carried out using forming gas ($10\%H_2/90\%N_2$). In a second run using the same conditions but about 10 wt% of Pt powder was added to the KNO_3 sample. A weight loss of about 13 % for the KNO_3 content is observed. There is a strong exothermic peak centered around 150°C due to the reaction related to the weight loss. The endothermic peak due to the structural phase transition appears only as a very small minima in the heating up run and the reversal to the low temperature phase is absence indicating the complete chemical reaction of KNO_3. The exothermic peaks at 220°C and 180°C in the cooling run can be related to the chemical products. The results are in agreement with observations reported by [75]. Two important conclusions can be drawn: 1. The hydrogen leaving the sodalite crystals are in an activated form which is able to reduce the nitrate even in some distance to the crystals in the pressed pellet (KBr/NaCl) as used in the TIR experiments. 2.

Hydrogen can be brought into an activated form at temperature already as low as 150°C in the presence of Pt. Therefore this effect could be used to increase the appropriate partial pressure of activated hydrogen to stop or even reverse the reactions eq. 1-4. Conclusively series of experiments were carried out using Pt powder in addition to the sample either brought in simply as additive to the powdered sample or even as additive in the synthesis route. Some main results may be outlined in the following.

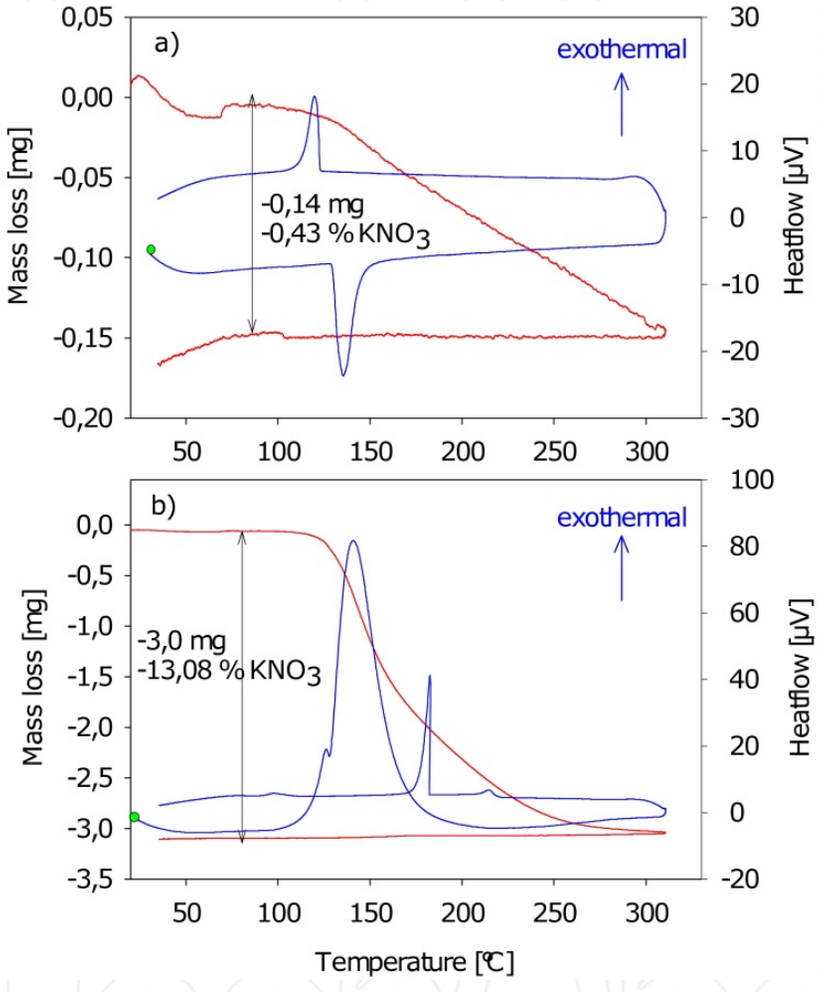

Figure 27. TG/DTA results of heating cooling cycles of KNO_3 powder without (a) and with the addition of Pt powder in flowing forming gas (10/90 H_2/N_2, 50 ml/min, 5°C/min).

First steps of experiments were carried out with the as synthesized BH_4-sodalite in comparison to samples with the addition of about 20 wt% Pt powder using various gases: He (99.9999), synthetic air (80%N_2/20%O_2) and forming gas (10%H_2/90%N_2). The experiments were carried out using always the same conditions with a continuous gas flow of 20 ml/min with heating rate of 4°C/min to 500°C, holding time of 10 min at 500°C, followed by cooling with 4°C/min to room temperature. Spectra of the starting sample and taken after the experiment are compared in Fig. 28. As before the heat treated samples reveal in all cases a reduction in BH_4-absorption intensity and peaks A, B, B' and C as related to $H_3B(OH)$-, $H_2B(OH)_2$-, $HB(OH)_3$- and BO_2-anion species, respectively. A quantification of the intensity ratio of BH_4^-/BO_2^- and the obtained mass losses with respect to the amount of BH_4-

sodalite is given in Tab. 4. These data sensitively show that the highest reaction rate is achieved under synthetic air conditions – and here to a higher extend in the presence of Pt compared to those in its absence. There is also a slightly lower weight loss in the presence of Pt indicating that here more hydrogen could have been released and less much loss to dehydration occurred. It may, however, also not be ruled out that any uptake of oxygen from the air occurred which could also be indicated by the increased intensity at the B peak position. Moreover the experiments show that the same weight losses and reaction rates BH_4^- to BO_2^- could be seen when He is used with and without Pt addition as well as forming gas only without Pt. If Pt is added the reaction rate becomes smaller and the weight loss increases. This shows that here dehydration takes place with a significantly reduced release of hydrogen. These preliminary experiments show the influence of hydrogen only in the presence of an effective activation of hydrogen which may produce a significant reduction in the concentration gradient for outward diffusion of H-anions.

Sample name	BH_4^-/BO_2^- ratio	Mass loss, Pt-influence subtracted [%]
500°C air, Pt	6,24	1,52
500°C air, no Pt	9,77	1,58
500°C He, Pt	18,35	1,79
500°C He, no Pt	19,81	1,79
500°C H_2/N_2, Pt	18,24	1,76
500°C H_2/N_2, no Pt	10,77	1,99

Table 4. Results of BH_4^-/BO_2^- ratio of integrated intensities from spectra shown in Fig. 28 and mass loss from TG experiments (heating up to 500°C) of a micro-crystalline BH_4-aluminosilicate sodalite sample with and without the addition of Pt powder

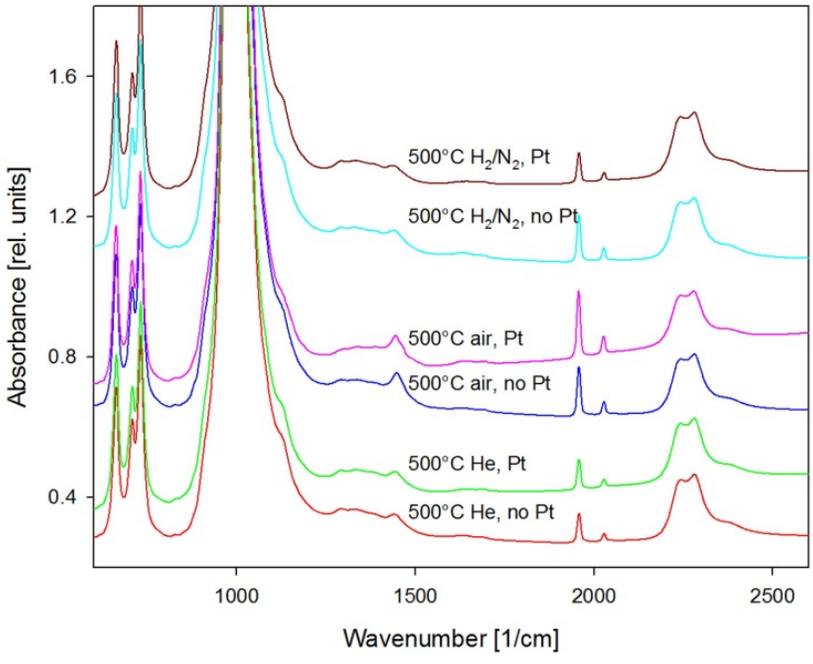

Figure 28. IR absorption spectra of thermally treated micro crystalline BH_4-aluminosilicate sodalite sample with and without the addition of Pt powder under various flowing gas compositions (for details see text).

Further experiments were carried out with BH_4-sodalites with Pt added into the synthesis route. X-ray diffraction pattern could prove the growth of microcrystalline BH_4-sodalite in the presence of nanocrystalline Pt. REM/EDX investigations show a rather homogeneous distribution of Pt. The IR spectra (see below) showed some weak formation of A peaks ($H_3B(OH)$-anion) due to the presence of Pt during synthesis. Typical results of the Pt free and Pt containing as synthesized samples treated with a hydrogen pressure of 162 bar and 3 h holding time at 250°C are shown in Fig. 29. The Pt free sample shows pronounced formation of peaks A and B related to $H_3B(OH)$- and $H_2B(OH)_2$-anions in the sodalite cages, respectively. Contrary to this the sample containing Pt shows almost no change in the infrared absorption beside only a slight increase in A peak intensity. It is interesting to note that there is no peak B′ observed. This can be explained by the too low temperature, but could also be related to the special high pressure conditions. It was observed using closed Au capsules and at 450°C for half an hour pre-reacted samples that the B′ peak completely disappeared at 300°C at autogeneous pressure. This implies a high stability for $H_3B(OH)$- and $H_2B(OH)_2$-anions but less much for $H_3B(OH)$-anions and also for dehydrated BO_2-anions under such conditions. As there is also no indication of $BO(OH)_2$-anions it may be concluded here that the peak at 3620-3640 cm^{-1} could be related to $B(OH)_4$-type species present already in the as synthesized sample.

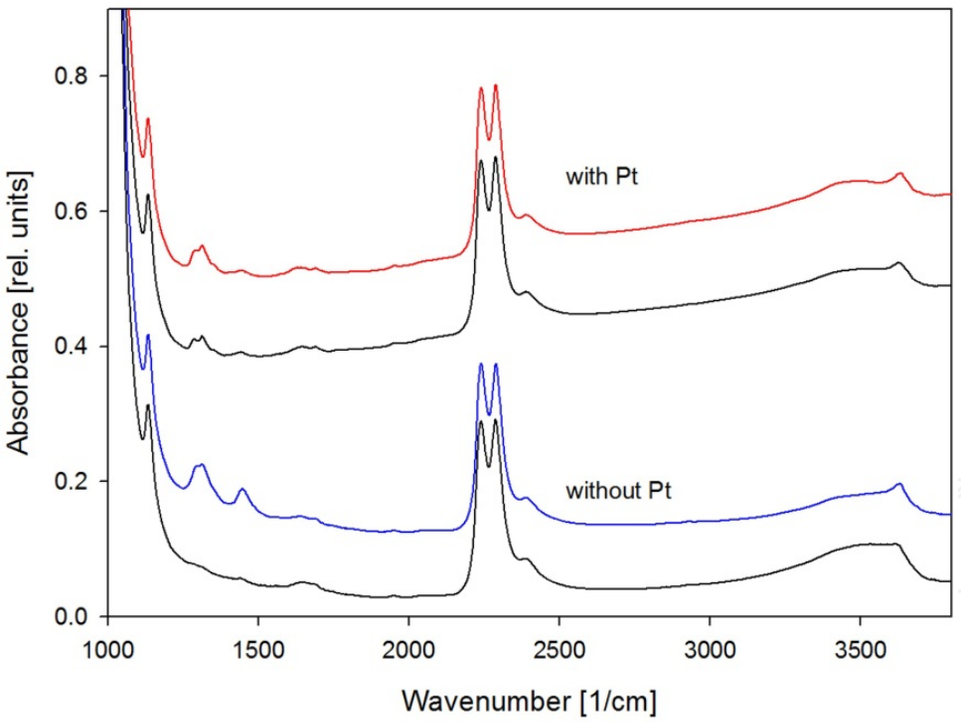

Figure 29. IR absorption spectra of microcrystalline BH_4-aluminosilicate sodalite sample with and without the addition of Pt during synthesis before (lower curve) and after (upper curve) treated for 3 h in 160 bar H_2 at 250°C (compare text).

In Fig. 30 the result of a reinsertion experiment carried out using 160 bar H_2 at 200°C of the Pt containing sample which was pre-reacted at 400°C in air is shown [25]. It can be seen that peak A increases in intensity whereas peak B decreases.

This first step of hydrogen reinsertion concerning the reaction eq. 2 could be supported in further systematic experiments where the influence of reaction temperature and time has been investigated at 55 bar hydrogen pressure on the Pt-containing sample pre-reacted at 400°C for 1 h. The results showed that with increasing temperature at 200, 250 and 300°C the BH_4-anion concentration remains constant and the same as in the pre-reacted sample. The A peak increases in intensity by about 10%, whereas the B peak decreases by about 5%. Moreover the $B(OH)_4^-$ related intensity did not vary within the error of estimation. Thus it is likely that under such conditions reaction eq. 2 could effectively be reversed. The evaluation of peak intensities with increasing reaction time at 250°C and 55 bar H_2 between minutes up to 6 h also showed that the BH_4-anion concentration remains rather constant also reproducing the finding of the former series. The content of $H_3B(OH)$-anions is higher compared to the pre-reacted material in minutes and slightly increases with increasing time. This shows that a fast reversion of reaction eq. 2 can be achieved.

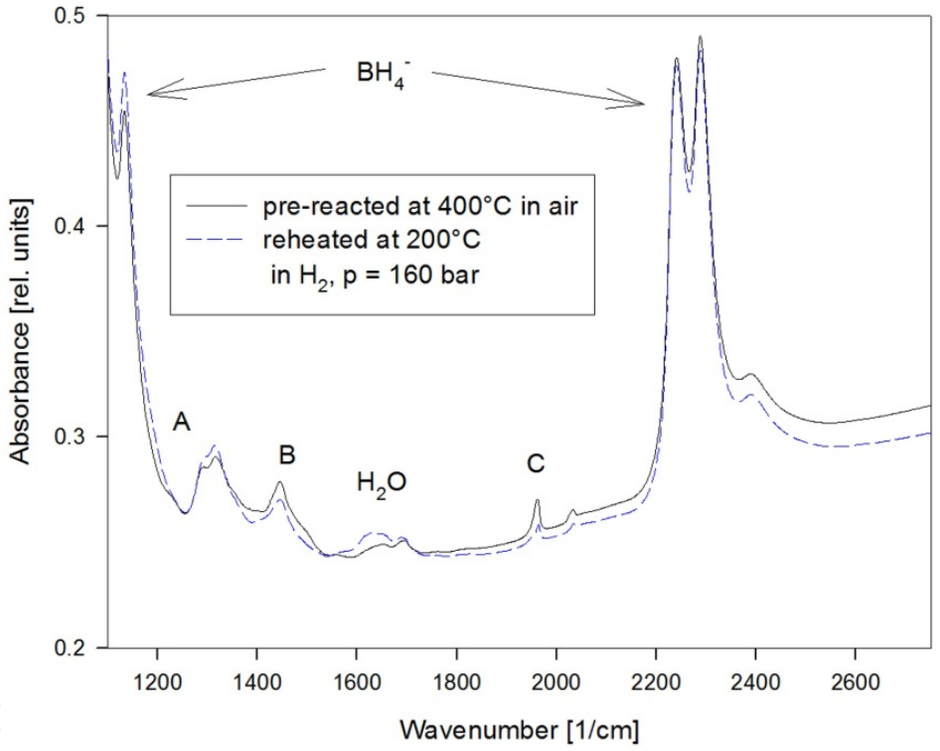

Figure 30. IR absorption spectra of microcrystalline BH_4-aluminosilicate sodalite sample with addition of Pt pre-reacted for 1 h at 400°C in air and reheated for 3 h in 160 bar H2 at 200°C, after [25] (compare text).

The reinsertion experiments have shown that a slight but significant back reaction in the content of $H_2B(OH)_2$-anions to $H_3B(OH)$-anions could be achieved. A higher efficiency might be reached with a further optimisation of the catalyst function. An improved back reaction might also be expected with the help of MgH_2 addition, which could increase the concentration gradient of H^- significantly. In some preliminary experiments commercially available 30 wt% MgH_2 powder (Merck) was simply mixed with two different pre-reacted samples and the spectra were taken of these samples and those after 3 h exposure to 150 bar hydrogen pressure at 200°C. The spectra shown in Fig. 31 reveal first of all the strong

contribution of MgH_2 which can be seen by direct comparison with the spectrum of MgH_2 also shown. The special pre-reaction conditions of the Pt-containing BH_4-sodalite are 4 h at 360°C (sample I) and 1 h at 450°C (sample II). The most obvious and important observations here are that in both cases some part of MgH_2 forms $Mg(OH)_2$ as is identified by the new sharp peak at 3699 cm^{-1} for the samples treated in 150 bar hydrogen. The evaluation of the intensity of the triplicate BH_4-peaks reveal an increased intensity by about 4 % and 2 % for sample I and II, respectively. By the same time the A-peak intensity decreased by about 6.2 % in both cases. These results indicate the formation of BH_4-anions in the sodalite cages according to eq. 1.

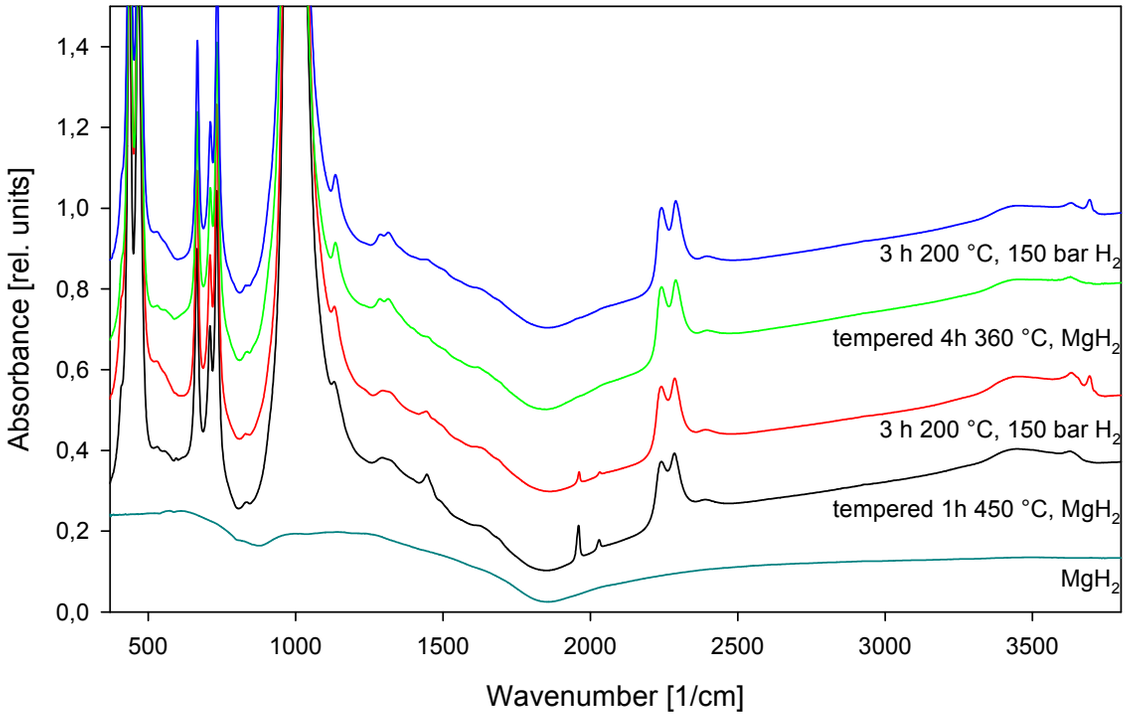

Figure 31. IR absorption spectra of microcrystalline BH_4-aluminosilicate sodalite sample pre-reacted, then mixed with 30 wt% MgH_2 and reheated (conditions as denoted). For comparison the spectrum for MgH_2 is also shown.

5. Summary and conclusion

Mixtures of $NaBH_4$ containing alkaline aluminate and silicate solutions form gels. During hardening at 110°C re-crystallization of $NaBH_4$ occurs together with the appearance of some sodalite type aluminosilicate within a remaining matrix of short range ordered sialate (Si-O-Al) bonds. The new material could easily be handled in water and at elevated temperatures up to about 300°C without significant destruction or release of hydrogen. Series of mixtures show that the aluminosilicate gel could contain up to 72 wt% of $NaBH_4$ content, which could totally be used for hydrogen release at room temperature by the addition of weak acid solutions. A further increase in effective $NaBH_4$ content could be obtained by reducing the temperature for hardening. Therefore, such type of handling of $NaBH_4$ could open new possibilities for future applications for the energy source hydrogen

Another new type of hydrogen storage is the encapsulation of the BH_4-anion in the sodalite cage revealing a whole family of compounds. Here the total content of the hydrogen is 10 times smaller compared to the pure $NaBH_4$-salt. However, it shows the big advantage that all the consecutive reaction steps for hydrogen release via the reaction with water could be discovered and mostly controlled. The hydrogen release reveals stepwise a zoned crystal system of $H_3B(OH)$-, $H_2B(OH)_2$-, $HB(OH)_3$- and $B(OH)_4$-anions in the sodalite cages. A dehydration of $B(OH)_4$-SOD to BO_2-SOD follows and could be controlled as well. It is very likely that hydrogen release from BH_4-sodalite resembles a diffusion controlled process with H^- and OH^- being the diffusing species. In section 4 experimental observations were given, supporting this interpretation. According to this it can be considered that H_2O becomes first dissociated and OH^- could exchange H^- in the cage, which recombines with H^+ to H_2. Conclusively first steps of a regeneration of the BH_4-anion could be obtained by realizing a diffusion gradient of H^- from outside to inside for pre-reacted BH_4-sodalite samples. It could be concluded that basically the Na-cations effectively close the sixring windows of the sodalite cages. With raising temperature above about 250°C there is an increasing probability of opening this window for an increasing ion exchange. Closing this window effectively protects the BH_4-anion from water attack. The absence of this effect in zeolite LTA for the grc- and toc-units thus could explain the failure of any successful stabilization of BH_4-anion or larger salt-type units in such frameworks. On the other hand for the BH_4-sodalite a further optimization of the reactor regeneration, e.g. by fine tuning of the geometrical parameter concerning the cage sizes as well as the distribution of the appropriate catalyst, for example the development of thin film technique, the BH_4-sodalite could gain some future application as hydrogen storage and hydrogen fuel processing from water.

Author details

Josef Christian Buhl, Lars Schomborg and Claus Henning Rüscher
Institut für Mineralogie, Leibniz Universität Hannover, Hannover

Acknowledgement

Some results were obtained with the financial support for students by the "Land Niedersachsen" and by fund of the Leibniz University of Hannover. Results obtained by LS could be reported prior to publication in his PhD thesis work.

6. References

[1] Bogdanivic B, Schwickardi (1997) M Ti-doped alkali metal aluminium hydrides as potential novel reversible hydrogen storage material. J. Alloys Compd., 253: 1-9.
[2] Schlapbach L, Züttel (2001) A Hydrogen storage materials for mobile applications. Nature 414: 353-358.
[3] Pradhan B K, Harutyunyan A R, Stojkovic D, Grossman J C, Zhang P, Cole M W, Crespi V H, Goto H, Fujiwara J, Eklund P C (2002) Large Cryogenic Storage of Hydrogen in Carbon Nanotubes at Low Pressures. J. Mat. Res. 17: 2209-2216.

[4] Hu Y H, Ruckenstein E (2006) Clathrate hydrogen hydrate – A promising material for hydrogen storage. Angew. Chem. Int. Ed. 45: 2011-2013.
[5] Schüth F (2006) Mobile Wasserstoffspeicher mit Hydriden der leichten Elemente. Nachrichten aus der Chemie 54: 24-28.
[6] Jia C, Yuan X, Ma Z (2009) Metal-organic frameworks (MOFs) as hydrogen storage materials. Prog. in Chem. 21: 1954-1962.
[7] Kuppler R J, Timmons D J, Fang Q-R, Li J-R, Makal T A, Young M D, Yuan D, Zhao D, Zhuang W, Zhou H-C (2009) Potential applications of metal-organic frameworks. Coordination Chemistry Reviews 253: 3042-3066.
[8] Murray L J, Dinca M, Long J R (2009) Hydrogen in metal-organic frameworks. Chem. Soc. Rev. 38: 1294-1314.
[9] Sculley J, Yuan D, Zhou H-C (2011) The current status of hydrogen storage in metal-organic frameworks updated. Energy Environ. Sci. 4: 2721-2735.
[10] Davis R E, Bromels E, Kibby Ch L (1962) Boron hydrides. III. Hydrolysis of sodium borohydride in aqueous solution. J. Am. Chem. Soc. 84: 885-892.
[11] Li Z P, Liu B H, Arai K, Morigazaki N, Suda S (2003) Anodic Oxidation of Alkali Borohydrides Catalyzed by Nickel. J. Alloys Compd. 356-357: 469-474.
[12] Liu B H, Li Z P (2009) Hydrogen generation from borohydride hydrolysis reaction J. Power Sources 187 (2): 527-534.
[13] Cao D, Chen D, Lan J, Wang G (2009) An alkaline $NaBH_4$-H_2O_2 fuel cell with high power density. J. Power Sources 190: 346-350.
[14] Buhl J-Ch (2011) Synthesis and properties of $NaBH_4$-imbibed aluminosilicate gels and its partial crystalline secondary products. Z. Kristallogr. Supplement Issue No. 31: 23-24.
[15] Schomborg L, Rüscher C, Buhl J-C (2012) Thermal Stability and quantification of hydrogen release of $NaBH_4$ enclosed in aluminosilicate gels. Z. Kristallogr. Suppl. Issue No. 32: 62
[16] Barrer R M (1982) Hydrothermal chemistry of zeolites. London: Academic Press. 348 p.
[17] Buhl J-Ch, Gesing T M, Rüscher C H (2005) Synthesis, crystal structure and thermal stability of tetrahydroborat sodalite $Na_8[AlSiO_4]_6(BH_4)_2$. Micropor. Mesopor. Mater. 80: 57-63.
[18] Buhl J-Ch, Gesing T M, Höfs T, Rüscher C H (2006) Synthesis and crystal structure of gallosilicate- and aluminogermanate tetrahydroborate sodalites $Na_8[GaSiO_4]_6(BH_4)_2$ and $Na_8[AlGeO_4]_6(BH_4)_2$. J. Solid State Chem. 179: 3877-3882.
[19] Höfs T K (2009) Synthese und thermisches Reaktionsverhalten $NaBH_4$-haltiger Sodalithe mit alumosilikatischem, gallosilikatischem und alumogermanatischem Strukturgerüst. Theses, Institute of Mineralogy, Leibniz University Hannover, Hannover.
[20] Höfs T K, Buhl J-Ch (2011) Thermal behavior of $NaBH_4$-sodalites with alumosilicate framework: Influence of cage water content and the surrounding conditions. Mat. Res. Bull. 46: 1173-2178.
[21] Poltz I, Robben L, Buhl J-Ch, Gesing T M (2011) Synthesis, crystal structure and high temperature behaviour of gallogermanate tetrahydroborate sodalite $Na_8[GaGeO_4]_6(BH_4)_2$. Z. Kristallogr. Suppl. Issue No. 31: 103.

[22] Buhl J-Ch, Schomborg L, Rüscher C H (2010) Tetrahydroborate sodalite nanocrystals: Low temperature synthesis and thermally controlled intra cage reactions for hydrogen release of nano- and micro crystals. Micro. Meso. Mater. 132: 210-218.
[23] Buhl J-Ch, Rüscher C H Schomborg L, Stemme F (2010) Nanocrystalline $NaBH_4$-enclathrated zeolite SOD: a model for improvement of safeness and reactivity of boron hydride based hydrogen storage systems. Clean Technology, www.ct-si.org, ISBN 978-1-4398-3419-0
[24] Rüscher C H, Stemme F, Schomborg L, Buhl J-Chr (2010) Low temperature hydrogen release from borontetrahydride-sodalite and ist reloading: Observations in in-situ and ex-situ TIR experiments Ceramic Transactions 215: 65-70.
[25] Schomborg L, Rüscher C H, Buhl J-Ch (2011) Hydrogen release and reinsertion reactions in $(BH_x$-$(OH)_y$-$O_z)$-SOD zoned crystal systems. Z. Kristallogr. Suppl. Issue 31: 24.
[26] Rüscher C H, Mielcarek E, Lutz W, Jirasit F, Wongpa J (2010) New insights on geopolymerisation using molybdate, Raman and infrared spectroscopy. Ceramic Engineering and Science Proceedings 31: 19-35
[27] Hermeler G, Buhl J-Ch, Hoffmann W (1991) The influence of carbonate on the synthesis of an intermediate phase between sodalite and cancrinite. Catalysis Today 8 415-426.
[28] Waddington T C (1958) Thallous borohydride $TlBH_4$. J. Chem. Soc.: 4783-4784.
[29] Goubeau J, Kallfass H (1959) Die Reaktion von Natriumborhydrid und Wasser. Z. Anorg. Allg. Chem. 299: 160-169.
[30] Schutte C J H (1960) The infra-red spectrum of thin films of sodium borohydride. Spectrochim. Acta 16: 1054-1059.
[31] Ketelaar J A A, Schutte C J H (1961) The boronhydride ion (BH_4^-) in a face centered cubic alkali-halide salt. Spectrochim. Acta 17: 1240-1243.
[32] Filinchuk Y, Hagemann H (2008) Structure and Properties of $NaBH4{\cdot}2H_2O$ and $NaBH_4$. Europ. J. Inorganic Chemistry 20: 3127-3133
[33] Hisatsune I C, Suarez N H (1964) Infrared Spectra of Metaborate Monomer and Trimer Ions. Inorg. Chem. 3: 168-174.
[34] Kessler G, Lehmann H A (1965) IR-spektroskopische Untersuchungen an Boraten: I. Natrium(1:1:4)borathydrat. Z. Anorg. Allg Chem. 338: 179-184.
[35] Pietsch H H E, Fechtelkord M, Buhl J-Ch (1997) The formation of unusual twofold coordinated boron in a sodalite matrix, J. Alloys Compd. 257: 168.
[36] Nakamoto K (1978) Infrared and Raman Spectra of Inorganic and Coordination Compounds. New York: John Wiley & Sons. 400 p.
[37] Weidlein J, Müller U, Dehnicke K (1981) Schwingungsfrequenzen I. Stuttgart/New York: Georg Thieme Vlg. 339 p.
[38] Rüscher C H (2005) Chemical reactions and structural phase transitions of sodalites and cancrinites in temperature dependent infrared (TIR) experiments. Microp. Mesop. Materials 86: 58-68.
[39] Davis R E, Swain C G (1960) The general acid catalysis of the hydrolysis of sodium borohydride. J. Am. Chem. Soc. 82: 5949-5950.
[40] Weitkamp J, Fritz M, Ernst S (1995) Zeolites as media for hydrogen storage. J. Hydrogen Energy 20: 967-970.

[41] Baur W H, Fischer R X (2008) A historical note on the sodalite framework: The contribution of Frans Maurits Jaeger. Microp. Mesopor. Mater. 116: 1-3.
[42] Fischer R X, Baur W H (2008) Symmetry relationships of sodalite (SOD) – type crystal structures. Z. Kristallogr. 224: 185-197.
[43] Johnson G M, Mead P J, Weller M T (2000) Synthesis of a range of anion-containing gallium and germanium sodalites. Microp. Mesopor. Mater. 38: 445-460.
[44] Wiebcke M, Sieger P, Felsche J, Engelhardt G, Behrens P, Schefer J (1993) Sodium Aluminogermanate Hydroxosodalite Hydrate $Na_{6+x}[Al_6Ge_6O_{24}](OH)X{\cdot}nH_2O$(X-Approximate-to-1.6, n-Approximate-to-3.0) - Synthesis, Phase Transitions and Dynamical Disorder of the Hydrogen Dihydroxide Anion, $H_3O_2^-$, in the Cubic High-Temperature Form. Z. Anorg. Allg. Chem. 619: 1321-1329.
[45] Gesing T M (2007) Structure and properties of tecto-gallosilicates II. Sodium chloride, bromide, bromide and iodide sodalites. Z. Kristallogr. 222: 289-296.
[46] Liebau F (1983) Zeolites and clathrasils-Two distinct classes of framework silicates. Zeolites 3: 191-193.
[47] Weller M T, Dodd S M, Myron Jiang M R (1991) Synthesis, structure and ionic conductivity of nitrite sodalite. J. Mater. Chem. 1: 11-15.
[48] Buhl J-Ch, Mundus C, Löns J, Hoffmann W (1994) On the enclathration of NaB(OH)4 in the ß-cages of sodalite: crystallization kinetics and crystal structure. Z. Naturforsch. 49a: 1171-1178.
[49] Buhl J-Ch, Gesing T M, Gurris C (2001) Synthesis and crystal structure of rhodanide-enclathrated sodalite $Na_8[GaSiO_4]_6(SCN)_2$. Micropor. Mesopor. Mater. 50: 25-32.
[50] Rüscher C H, Gesing T M, Buhl J-Ch (2003) Anomalous thermal expansion behaviour of $Na_8[AlSiO_4]_6(NO_3)_2$-sodalite: P4-3n to Pm3-n phase transition by untilting and contraction of TO_4 units Z. Kristallogr. 218: 332-344.
[51] Mikheeva V I, Bredtsis V B (1960) Solubility isotherm for sodium boron hydride and sodium hydroxyde in water at zero degrees. Dokl. Akad. Nauk SSSR 131: 1349-1350.
[52] Mesmer R E, Jolly W L (1962) Hydrolysis of aqueous hydroborate. Inorg. Chem. 1 (3): 608-612.
[53] Hadan M, Fischer F (1992) Synthesis of fine grained NaA-type Zeolites from superalkaline solutions. Cryst. Res. Technol. 27: 343-350.
[54] Fischer F, Hadan M, Fiedrich G (1992) Zeolite syntheses from superalkaline reaction mixtures. Collect. Czech. Chem. Commun. 57: 788-793.
[55] Fan W, Morozumi K, Kimura R, Yokoii T, Okubo T (2008) Synthesis of nanometer-sized sodalite without adding organic additives. Langmuir 24: 6952-6958.
[56] Mashal K, Harsh J B, Flury M, Felmy A R (2005) Analysis of precipitates from reactions of hyperalkaline solutions with soluble silica. Appl. Geochem. 20: 1357-1367.
[57] Wang L Q, Mattigod S V, Parker K E, Hobbs D T, McCready D E (2005) Nuclear magnetic resonance studies of aluminosilicate gels prepared in high-alkaline and salt-concentrated solutions. J. Non-Cryst. Solids 351: 3435-3442.
[58] Abts L M, Langland J T, Kreevoy M M (1975) Role of water in hydrolysis of BH_4^-. J. Am. Chem. Soc. 97 (11): 3181-3185.

[59] Fleet M E (1989) Structures of sodium alumino-germanate sodalites [$Na_8(Al_6Ge_6O_{24})A_2$, A = Cl, Br, I]. Acta. Cryst. C45: 843-847.

[60] Flanigen E M, Khatami H, Szymanski H A (1971) Infrared structural studies of zeolite frameworks. Advan. Chem. Ser. 101: 201-209.

[61] Löns J, Schulz H (1967) Strukturverfeinerung von Sodalith $Na_8Si_6Al_6O_{24}Cl_2$. Acta Cryst. 23: 434-436.

[62] Davis R L, Kennard C H L (1985) Structure of sodium tetradeutoroborate, $NaBD_4$. J. Solid State Chem. 59: 393-396.

[63] Izumi F (1993) Rietveld analysis programmes Rietan and Premos and special applications. In: Young R A, editor. The Rietveld Method. Oxford: Oxford University Press. pp. 236-253.

[64] Marcus M, Bredow T, Schomborg L, Rüscher C H, Buhl J-C (2012) Structure and IR spectra of $Na_8[AlSiO_4]_6(BH_4)_2$ sodalite: Comparison between theoretical predictions and experimental data. Z. Kristallogr. Suppl. Issue No. 32: 89-90

[65] Buhl J-Ch, Murshed M-M (2009) $(Na_4BH_4)^{3+}$ guests inside aluminosilicate, gallosilicate and aluminogermanate sodalite host frameworks studied by 1H, 11B, and 23Na MAS NMR spectroscopy. Mat. Res. Bull. 44: 1581-1585.

[66] Wrackmeyer B (1988) NMR Spectroscopy of Boron Compounds Containing Two-, Three- and Four-Coordinate Boron Ann. Rep. NMR Spectrosc. 20: 61-203.

[67] Bray P J (1999) NMR and NQR studies of boron in vitreous and crystalline borates. Inorg. Chim. Acta 289: 158-173.

[68] Hansen M R, Madsen G K H, Jakobsen H J, Skibsted J (2005) Refinement of borate structures from 11B MAS NMR spectroscopy and density functional theory calculations of 11B electric field gradients. J. Phys. Chem. A 109: 1989-1997.

[69] Buhl J-Ch, Engelhardt G, Felsche J (1989) Synthesis, X-ray diffraction and MAS n. m. r. characteristics of tetrahydroxoborate sodalite, $Na_8[AlSiO_4]_6$ $[B(OH)_4]_2$. Zeolites 9: 40-44.

[70] Massiot D, Fayon F, Capron M, King I, Le Calve S, Alonso B, Durand J, Bujola B, Gan Z, Hoatson G (2002) Modelling one- and two-dimensional solid state NMR spectra. Mag. Res. Chem. 40: 70-76.

[71] Engelhardt G, Sieger P, Felsche J (1993) Multinuclear solid state NMR of host-guest systems with TO_2 (T=Si, Al) host-frameworks. A case study on sodalites. Analytica Chimica Acta 283: 967-985.

[72] Pietsch H-H E, Fechtelkord M, Buhl J C (1992) The formation of unusually twofold coordinated boron in sodalite matrix. J. Alloys and Compounds 257: 168-174

[73] Fechtelcord M (2000) Influence of sodium ion dynamics on the ^{23}Na quadrupolar interaction in sodalite: A high temperature ^{23}Na MAS NMR study. Solid State Nucl. Magn. Res 18: 70-88

[74] Rüscher C H, Schomborg L, Buhl J-C (2010) Thermally Controlled Water Injection into BH_4-Sodalie for Hydrogen Formation Investigated by IR Absorption. Diffusion Fundamentals 12: 37-39

[75] Phair J W (2007) Stability of alkali nitrate/Pd composites for hydrogen separation membranes. Energy and Fuels Vol. 21 Issue 6: 3530-3536